POWER SYSTEM TRANSIENT STABILITY ANALYSIS CONSIDERING LOAD AND WIND POWER GENERATION VARIABILITY

Prepared by: Siyanda Ncwane

Supervised by: Professor Komla A. Folly

June 2023

Submitted to the Department of Electrical Engineering at the University of Cape Town in partial fulfilment of the academic requirements for a Master of Science in Electrical Engineering

University of Cape Town

The copyright of this thesis vests in the author. No quotation from it or information derived from it is to be published without full acknowledgement of the source. The thesis is to be used for private study or non-commercial research purposes only.

Published by the University of Cape Town (UCT) in terms of the non-exclusive license granted to UCT by the author.

University of Cape Town

Declaration

I know the meaning of plagiarism and declare that all the work in the document, save for that which is properly acknowledged, is my own. This thesis/dissertation has been submitted to the Turnitin module (or equivalent similarity and originality checking software) and I confirm that my supervisor has seen my report and any concerns revealed by such have been resolved with my supervisor.

Student Name : Siyanda Ncwane

Signature : Signed by candidate

Date : 12/06/2023

ACKNOWLEDGEMENTS

I would like to thank Professor Komla Folly for supervising this research. His inputs greatly improved my comprehension of research and the research process. I would also like to thank my family, friends, and colleagues for their support during the period I worked on this research.

ABSTRACT

This research investigated the transient stability of a power system that integrated wind power generators (WPGs) by considering the variability of the system load and power they produced. The power produced by the WPGs was modelled using wind speed, while the variability of the power system load and wind speed was modelled using distribution functions. Power system transient stability was investigated using the deterministic and probabilistic methods. The deterministic method was used to investigate the power system transient stability based on 9 scenarios consisting of low, moderate, and peak system loading and wind power generation conditions. The probabilistic method was also used to investigate power system transient stability using scenarios consisting of low, moderate, and peak system loading conditions. During each of the three system loading conditions, the variable power produced by the WPGs was modelled using 5000 samples that were randomly sampled using Monte-Carlo Simulations. It was found that selecting distribution functions based on their fit alone did not ensure that they modelled the load and wind speed range. Their data range modelling ability ensured that they synthesised the low and high load and wind speed values. It was also found through power system simulations that the transient stability was negatively impacted when the power system's net-load reduced because of increased wind power generation penetration levels. These findings highlight that distribution functions should not be selected based only on their fit to load and wind speed data. In addition to a good fit, they should also be assessed to determine whether they synthesise the data range. The research findings also highlight that power system transient stability should be investigated using scenarios in which the power produced by WPGs is high, during periods when the system's net-load is low.

TABLE OF CONTENTS

LIST OF FIGURES

LIST OF TABLES

LIST OF ABBREVIATIONS

B-splines	Basis splines
CDF	Cumulative distribution function
ECDF	Empirical cumulative distribution function
GMM	Gaussian mixture model
GW	Gigawatt
IEC	International Electrotechnical Commission
IEEE	Institute of Electrical and Electronics Engineers
KDE	Kernel density estimation
LHS	Latin hypercube sampling
LDE	Logspline density estimation
MCS	Monte-Carlo Simulations
ms	Millisecond
MW	Megawatt
PDF	Probability distribution function
pu	Per unit
RES	Renewable energy sources
s	Second
SDGs	Sustainable development goals
SCO	Synchronous condenser operation
WPGs	Wind power generators

CHAPTER 1: INTRODUCTION

1.1. Background

Society's increased awareness of the environmental impacts of generating energy from fossil fuels has necessitated the increased generation of energy from renewable energy sources (RES). The United Nations' 2030 sustainable development goal (SDG) number 7, which is to "ensure access to affordable, reliable, sustainable and modern energy for all", promotes increasing the share of energy produced from RES such as wind and solar [1]. One of the initiatives to increase the production of energy from RES in power systems is through integrating wind power generators (WPGs). The 2022 Global Wind Report indicates that at the end of 2021, the total capacity of WPGs integrated to power systems was 837 GW [2]. The increased integration of WPGs will impact the transient stability because they change the dynamic operating conditions of power systems.

1.2. Research motivation

Prior to the introduction of RES, power systems had centralised generation and distributed loads. In a centralised generation power system, the power was transferred from the generation sources to the loads. The integration of RES results in the decentralisation of generation owing to the distributed nature of resources. WPGs have been integrated to several power systems to increase the generation of power from wind. The deterministic method, which entails modelling the load and power produced by WPGs as a percentage of their peak demand and of their capacity, respectively, has been used in several studies to investigate the impact of WPGs on power system transient stability [3-6]. A limitation of the deterministic method is that it does not account for the impact of the variable power system operating conditions on transient stability [5-8].

An increased adoption of the probabilistic method is required to account for the impact of the variable power system operating conditions on transient stability. The probabilistic method, which entails accounting for the variability of system load and power produced by WPGs has been used in several studies to investigate the transient stability of power

systems integrating WPGs and to assess numerous power system operating conditions [9-13]. The increased penetration of WPGs increases the variability of power systems owing to the variable power they produce.

1.3. Research objective

The research objective was to investigate the impact of load and power produced by WPGs on power system transient stability. This research investigated whether it would be sufficient to select distribution functions based only on their fit as opposed to also selecting them based on their ability to synthesise the load and wind speed range. The power produced by the WPGs was developed using wind speed. The load used in the research was measured from three substations supplying residential load in South Africa. The wind speed was measured from three wind speed measurement sites in South Africa. Both the load and wind speed were randomly sampled using Monte-Carlo Simulations to develop samples to perform probabilistic power system transient stability studies. The power system's transient stability was investigated using deterministic and probabilistic methods.

1.4. Research contributions

The research performed showed that selecting distribution functions based on their fit to load and wind speed does not ensure that they model the data range. This may result in the synthesised load being unable to model low and peak system loading conditions. Also, this may result in the synthesised wind speed when converted to power being unable to model the low and peak power produced by the WPGs. Furthermore, the research performed showed that increasing the penetration level of WPGs reduced the system's net load, resulting in reduced power system transient stability. This indicates that the transient stability of power systems integrating WPGs should be investigated using system operating conditions where the power produced by WPGs is high while the system net-load is low.

1.5. Research scope and limitations

This research investigated the transient stability of a power system by taking into account the variability of the load and power produced by WPGs. The IEEE 9-bus test system was used as a case study. Three WPGs were integrated into the test system. The variability of the load and power produced by the WPGs was modelled using the measured load and wind speed from three South African substations and wind speed measurement sites. Distribution functions were fitted to the measured load's and wind speed's to determine which were suitable for modelling the load and wind speed's variability. The research limitation is that the power produced by WPGs was developed by converting wind speed into the power they produced using a wind turbine power curve. This was done due to power production measurements from operating WPGs in South Africa being unavailable for use in this research.

The approach used in this research can be applied to any power system. However, the transient stability results presented in this research should not be generalised to other power systems. This is because power system transient stability is dependent on the system pre-fault operating conditions, the type of fault applied and the location of the fault. As a result, different power systems will behave differently during system faults.

1.6. Dissertation's layout

The dissertation is organised as follows:

- Chapter 2 presents a review of the literature on the transient stability of power systems integrating WPGs. The reviewed literature focuses on load and wind speed variability modelling, the assessment of the spatial correlation of power system variables, and the assessment of power system transient stability using deterministic and probabilistic methods.
- Chapter 3 presents the research methodology. The research process and methods used to perform probabilistic power system transient stability analysis are discussed. Also, the measurement uncertainty in the load and wind speed used in this research are discussed.
- Chapter 4 presents the power system equipment modelling and discusses the power system and WPGs dynamic models.

- Chapter 5 presents an investigation on load density modelling using distribution functions, as well as the impact of the modelled variable load on power system transient stability.
- Chapter 6 presents an investigation on wind speed density modelling using distribution functions. The variable power produced by WPGs that are integrated to a power system is developed using the wind speed. The impact on power system transient stability of the variable power produced by WPGs is also investigated in this chapter.
- Chapter 7 investigates power system transient stability using deterministic and probabilistic methods. The power system's low, moderate, and peak loading conditions are studied. During each power system loading condition, three scenarios of power produced by the WPGs are assessed using the deterministic method, while during each power system loading condition, 5000 scenarios of power produced by the WPGs are assessed using the probabilistic method.
- Chapter 8 presents the research's conclusions. It also discusses the research's findings, and proposes recommendations for future research.

CHAPTER 2: LITERATURE REVIEW

2.1. Introduction

As discussed in Chapter 1, wind power generation integration into power systems is increasing. In this chapter, the literature on the analysis of power system transient stability with wind power generators (WPGs) integrated is reviewed. The modelling of load and wind speed is reviewed first. Then the literature on methods used to assess the spatial correlation of power system variables is reviewed. Finally, the assessment of power system transient stability using the deterministic and probabilistic methods is reviewed.

2.2. Load modelling

2.2.1. Aggregated load modelling

In power system studies, load is represented by aggregated load models [14-16]. The aggregated load models can be static or dynamic [14, 16]. In studies investigating the impact of WPGs on power system transient stability, static models in which the load is modelled as a hybrid constant current, constant power, and constant impedance load have been used [17-19]. In other studies, loads have been modelled as a constant impedance [19, 20]. However, some studies have modelled loads using dynamic load models [15, 19]. When modelling dynamic loads, a composite load model that represents the aggregated static and dynamic components of the loads is used [15, 21]. The impact of load modelling on power system transient stability was investigated in [15, 16] using static and dynamic models. The authors in [15, 16] found that compared with static load models, using dynamic load models led to worse power system transient stability. This was because dynamic load models increase the time it takes for voltages to recover and stabilise after faults are isolated, causing power system voltages to be suppressed for a longer period compared to when static load models are used [15]. This results in reduced available network capacity to transfer the kinetic energy stored in the synchronous generator's (SG's) rotors during the period that faults are applied. The inability of the SGs to adequately export the energy stored in their rotors results in higher

rotor angle accelerations, which in turn cause larger rotor angle deviations. A limitation of using dynamic load models is that compared with static load models, they require additional computational resources, resulting in increased simulation times [16].

2.2.2. Load variability modelling

Loads impact the reliable operation of power systems because they affect power flows and voltage levels. In a power system, the load varies throughout the day because of changes in customer demand. The variability of the load is commonly modelled using distribution functions [22-24]. The parametric Gaussian, which models load density that is unimodal and is not skewed has been used in [22, 25, 26] to model load variability. Some studies have modelled the load density using the non-parametric Kernel density estimation (KDE) [23, 27] and the parametric Gaussian mixture model (GMM) [24, 28]. The benefits of modelling load density using the KDE and GMM over the Gaussian are that they can model densities that are skewed and multimodal [23, 24, 28]. The fit of the parametric GMM, Gaussian, log-normal, beta, and gamma to load density was investigated in [29]. Their ability to model the load density was evaluated using the chi-square (χ^2) statistic [29]. The investigation found that the GMM had a better fit to the load density than the Gaussian, log-normal, beta, and gamma. A limitation of the studies done in [22-29] was that the authors did not assess whether the distribution functions modelled the load range. As a result, it was not clear from these studies whether these distribution functions could model the load range. Their load range modelling ability ensures that the load they synthesise can be used to model power system low and peak demand conditions.

2.3. Wind power generation modelling

2.3.1. Aggregated wind power generator models

In WPGs, wind turbines are interconnected via a collector network to the grid integration step-up transformer [30-32]. WPGs can be modelled using either detailed or aggregated models. In detailed models, all of the equipment within WPGs is modelled, causing the algorithms used for simulations to be computationally intensive [31, 33]. On the other

hand, in aggregated models, the WPGs are modelled as parallel wind turbines, and the collector system cable network is ignored [30-34]. The impact of WPGs on power system transient stability is commonly investigated using aggregated WPG models [32, 35-37], while detailed models are commonly used to assess the performance of individual wind turbines within the WPG during power system faults [31, 34].

2.3.2. Wind speed variability modelling

Distribution functions such as the parametric Weibull [38-42], Rayleigh [38-42], Gamma [40, 41], Gumbel [40, 41], Gaussian [42], Wakeby [41, 43, 44], Kappa [41, 43, 44], and the non-parametric KDE [41, 42] have been used in several studies to model wind speed variability. Their fit to wind speed density has been evaluated using metrics such as the mean percentage error (MPE) [38], the mean absolute percentage error ($MAPE$) [38], the root mean square error ($RMSE$) [38, 40, 41], the mean absolute error (MAE) [41], the chi-square (χ^2) statistic [38, 41, 43], the coefficient of determination (R^2) [39-42, 44], the Kolmogorov-Smirnov (K-S) test statistic [41], and the Willmott index (d) [40]. In the studies performed in [38-40], the Weibull was found to fit wind speed better than the Rayleigh, Gamma, and Gumbel. However, the Wakeby and Kappa have been found to fit wind speed better that the Weibull [43, 44]. Unlike the Weibull whose shape is defined by two parameters, the shapes of the Wakeby and Kappa are defined by five and four parameters, respectively, allowing them to have a better fit to wind speed. Furthermore, the non-parametric KDE has been found to fit wind speed better than the parametric Gamma, Weibull, Gumbel, Rayleigh, Gaussian, Wakeby, and Kappa [41, 42] because its shape is not defined by parameters unlike the parametric distribution functions. A limitation of the studies performed in [38-44] was that the distribution functions' wind speed range synthesis ability was not assessed. In the literature that was reviewed, it was not clear whether the distribution functions that were assessed are capable of modelling the wind speed range. Distribution functions that can model the wind speed range are able to synthesise data that can model the full range of power produced by WPGs.

2.3.3. Conversion of wind speed to power

Wind speed is converted to the power produced by WPGs using wind turbine power curves. Figure 2.1 shows the shape of a typical wind turbine power curve [45, 46]. The power curve has four regions of operation. In region 1, the wind turbine does not produce power since the wind speed is less than the cut-in wind speed. In region 2, the power produced by the wind turbine increases as the wind speed increases. In region 3, the wind turbine's rated power is produced. In region 4, the wind turbine does not produce power to protect the machine from high wind speeds. The four regions of a wind turbine power curve can be modelled using piecewise mathematical modelling [10, 47, 48].

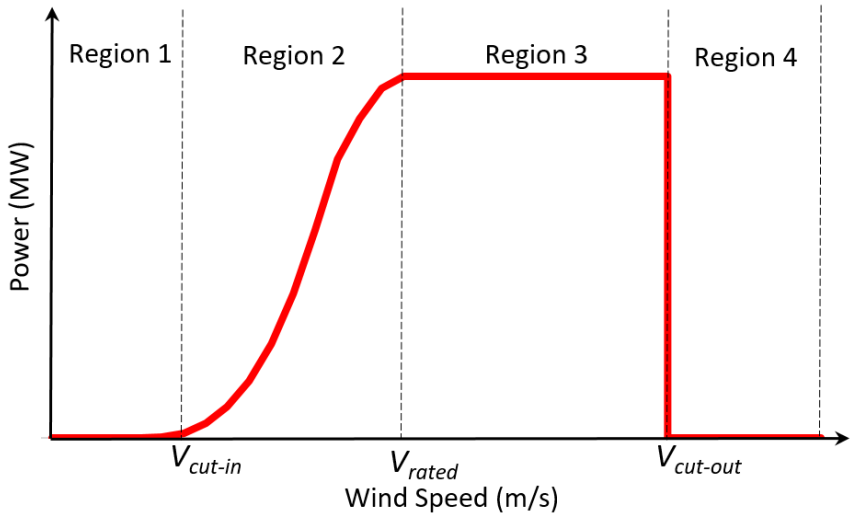

Figure 2.1: Wind turbine power curve

2.4. Spatial correlation of power system variables

The correlation among power system variables is evaluated using rank correlation [47, 49-51] and linear correlation [49, 52] coefficients. Rank correlation coefficients assess the non-linear correlation of power system variables [47, 49, 51], while the linear correlation coefficient assesses the linear correlation of the variables [47, 52, 53]. Rank correlation is evaluated using the Kendall's tau correlation coefficient [47, 49, 50] and the Spearman's correlation coefficient [47, 49, 51]. However, linear correlation is evaluated using the Pearson correlation coefficient [49, 52]. Unlike the linear correlation coefficient, rank correlation coefficients preserve the correlation when the data is transformed [54].

2.5. Power system transient stability

2.5.1. Deterministic method

The transient stability of power systems integrating WPGs has been investigated in several studies using the deterministic method [4, 5, 35, 55]. The studies have integrated WPGs consisting of wind turbines based on squirrel cage induction generators (SCIGs) [55], doubly-fed induction generators (DFIGs) [4, 5, 35, 55], and fully-rated converter generators [55]. The studies performed in [4, 5] investigated the impact of increasing the power produced by WPGs consisting of DFIG wind turbines on power system transient stability. It was found that increasing the power produced by WPGs, while maintaining the power produced by SGs constant, reduced the power system's transient stability [4, 5]. Also, in [5] it was found that increasing the power produced by a WPG while reducing the power produced by a SG improved the power system's transient stability. Reducing the power produced by SGs reduces the kinetic energy stored in their rotors during system faults. This results in improved power system transient stability because the SGs rotors accelerate less, resulting in lower rotor angle deviations during system faults. In [35], the number of WPGs consisting of DFIG wind turbines was increased in a power system. It was found that increasing the number of WPGs reduced the power system's transient stability [35]. A study performed in [55] investigated the transient stability of a power system using three scenarios in which a WPG consisting of SCIG, DFIGs, and fully-rated converter generator wind turbines was integrated. The number of turbines in the WPG was increased from one to five during the investigation [55]. It was found that when the WPG was equipped with fully-rated converter generator wind turbines, the power system had the best transient stability, followed by when the wind turbines were DFIGs, and, last, when the wind turbines were SCIGs [55]. WPGs consisting of SCIGs absorb reactive power when there are faults in the power system, resulting in reduced system voltages [55]. As a result, the power system has less capacity to transfer the kinetic energy stored in the SGs' rotors during the faults. On the other hand, WPGs consisting of DFIGs inject reactive power once the faults are isolated, helping to regulate voltages in the power system. WPGs consisting of fully-rated converter generator wind turbines inject reactive power both during power system faults and after the faults have been isolated, to improve voltages. A limitation of using the deterministic method is that

only a few system operating conditions are assessed. However, power systems have numerous operating conditions owing to the variability of load and power produced by the WPGs. Some of the numerous operating conditions can result in transient instability if faults occur in the power system.

2.5.2. Probabilistic method

Several studies have used the probabilistic method to investigate the transient stability of power systems that integrate WPGs [9-11, 56]. The studies have investigated power systems integrating WPGs consisting of DFIGs [9-11, 56] and fully-rated converter generators [9]. A study performed in [9] investigated the impact on power system transient stability of the variable power produced by a WPG consisting of DFIGs and fully-rated converter generators. It was found that when the WPG was equipped with fully-rated converter generators, the power system was more transiently stable than when it had DFIGs [9]. In WPGs consisting of DFIGs, to divert over-currents from the DFIGs' windings during system faults, DFIGs activate the crowbar system, disabling the generators' ability to inject reactive power [35, 37]. However, WPGs with fully-rated converter generators are able to support voltages by injecting reactive power both during and after power system faults have been isolated [57]. Transient stability is improved because the power system's transfer capacity is improved, thereby enabling SGs to expel quickly the kinetic energy stored in their rotors during the system faults. In [10], the deterministic and probabilistic methods were used to assess the impact on a power system's transient stability of the power produced by a WPG equipped with DFIGs. The investigation found that when using the deterministic method, increasing the power produced by the WPG resulted in the power system becoming transiently unstable [10]. However, using the probabilistic method showed that the power system was transiently unstable during 78% of the scenarios that were assessed [10]. Unlike the deterministic method, the probabilistic method assessed numerous power system operating conditions. As a result, the probabilistic method can be used to identify operating conditions in which a power system becomes transiently unstable. The authors in [11] used the probabilistic method to investigate the impact on power system transient stability of the power produced by WPGs consisting of DFIGs. It was found in [11] that increasing the power produced by the WPGs resulted in the increased probability that

the power system would become transiently unstable. In [56], the impact of a WPG consisting of DFIGs on a power system's transient stability was investigated by generating random values of the power it produced using Monte-Carlo Simulations (MCS) and the conditional probability theorem. It was found that compared with the conditional probability theorem, using MCS resulted in an optimistic probability of the power system remaining transiently stable [56]. A limitation of the studies performed in [9-11, 56] is that they focused on assessing the impact of the power produced by WPGs on transient stability, and did not consider the role played by the power system load.

2.6. Summary

The literature reviewed in this chapter showed that WPGs can be modelled using aggregated or detailed models. Also, power system load can be modelled using aggregated static or dynamic load models. It was found that dynamic load models are computationally intensive, resulting in increased power system simulation time. The literature review also suggested that the variability of load and wind speed is commonly modelled using distribution functions. It was found that distribution functions are commonly selected based on their fit to load and wind speed data, without considering whether they also model the data range. The literature review also showed that the transient stability of power systems that integrate WPGs can be assessed using the deterministic and probabilistic methods. It was also found that increasing the power produced by WPGs operates power systems closer to transient instability.

CHAPTER 3: METHODOLOGY

3.1. Introduction

In the previous chapter, the literature on the modelling of load and wind speed was reviewed. Also, the analysis of power system transient stability using the deterministic and probabilistic methods was reviewed. The research process and methods used in this research are discussed in this chapter. A quantitative research process is used in this research. The research process entails using distribution functions to model load and wind speed variability in a power system integrating wind power generators (WPGs). The variable power produced by the WPGs is developed using the wind speed. Power system transient stability is then assessed considering the variable load and power produced by WPGs.

3.2. Distribution functions

The substation load used in this study has been measured using three-phase four-wire statistical meters with a 0.5% active power measurement uncertainty, and a 1% reactive power measurement uncertainty. The wind speed used in this study has been measured using cup anemometers with a 1% wind speed measurement uncertainty, mounted at a height of 10 m on a mat mast. The measured load and wind speed densities are each modelled using seven distribution functions. The load density is modelled using the parametric Rayleigh, Gaussian, Wakeby, Gaussian mixture model (GMM) and Kappa, and the non-parametric Kernel density estimation (KDE) and Logspline density estimation (LDE). The wind speed density is modelled using the parametric Rayleigh, Weibull, Wakeby, Gumbel and Kappa, and the non-parametric KDE and LDE.

The Weibull probability distribution function (PDF) is given in equation (3.1) [39, 58].

$$f(v) = \frac{\delta}{\beta}\left(\frac{v}{\beta}\right)^{\delta-1} e^{-\left(\frac{v}{\beta}\right)^{\delta}} \tag{3.1}$$

where v is the modelled variable such as wind speed or load, and δ and β are the shape parameter and scale parameter, respectively.

The Rayleigh PDF is given below in equation (3.2) [59].

$$f(v) = \frac{v-\xi}{\beta^2} e^{\frac{-(v-\xi)^2}{2\beta^2}} \tag{3.2}$$

where v is the modelled variable such as wind speed or load, and β and ξ are the scale and location parameters, respectively.

The Gumbel PDF is given below in equation (3.3) [40, 59].

$$f(v) = \frac{e^{\frac{-(v-\xi)}{\beta}} e^{\left[-e^{\frac{-(v-\xi)}{\beta}}\right]}}{\beta} \tag{3.3}$$

where v is the modelled variable such as wind speed or load, and ξ and β are the location and scale parameters, respectively.

The Gaussian PDF is given below in equation (3.4) [59, 60].

$$f(v) = \frac{1}{\sigma\sqrt{2\pi}} e^{-\frac{(v-\mu)^2}{2\sigma^2}} \tag{3.4}$$

where v is the modelled variable such as wind speed or load, and σ and μ are the standard deviation and mean parameters, respectively.

The Wakeby PDF is given below in equation (3.5) [41, 43, 59].

$$f(v) = \left(\alpha[1-F(v)]^{\beta-1} + \gamma[1-F(v)]^{-\delta-1}\right)^{-1} \tag{3.5}$$

where v is the modelled variable such as wind speed or load, α and β are the first and second scale parameters, respectively, ξ is the location parameter, and γ and δ are the first and second shape parameters, respectively.

The Kappa PDF is given below in equation (3.6) [41, 43, 44, 61].

$$f(v) = \alpha^{-1}\left[1 - \frac{K(v-\xi)}{\alpha}\right]^{\frac{1}{K}-1} \times [F(v)]^{(1-h)} \tag{3.6}$$

where v is the modelled variable such as wind speed or load, α is the scale parameter, K and h are the first and second shape parameters, respectively, and ξ is the location parameter.

The GMM PDF is given below in equation (3.7) [60]. The GMM models data using a mixture of several Gaussian distribution functions.

$$f(v) = \sum_{i=1}^{N} \omega_i \frac{1}{\sigma_i\sqrt{2\pi}} e^{-\frac{(v-\mu_i)^2}{2\sigma_i^2}} \tag{3.7}$$

where v is the modelled variable such as wind speed or load, N is the number of Gaussian distribution functions used in the mixture model, ω_i, σ_i, and μ_i are the ith Gaussian distribution function's weight, standard deviation and mean, respectively.

The KDE PDF is given below in equation (3.8) [62-64]. The KDE's bandwidth is evaluated using equation (3.9) [41, 62, 63]. The KDE PDF fits Gaussian kernels given by equation (3.10) when modelling data [42, 62].

$$f(v) = \frac{1}{nh}\sum_{i=1}^{n} K\left(\frac{v-v_i}{h}\right) \tag{3.8}$$

$$h = \left(\frac{4}{3n}\right)^{\frac{1}{5}}\sigma \tag{3.9}$$

$$K(v) = \frac{1}{\sqrt{2\pi}} e^{-\frac{v^2}{2}} \tag{3.10}$$

where v is the modelled variable such as wind speed or load, n is the number of samples, K is a Gaussian kernel, h is the kernel bandwidth, σ is the standard deviation of the modelled variable, and v_i is the i^{th} measurement of the modelled variable.

The LDE PDF is given in equation (3.11) [65, 66]. The LDE PDF uses basis-splines (B-splines) to model data [66].

$$f(v) = e^{\sum_{n=1}^{n} \theta_n B_n(v) - C(\theta)} \tag{3.11}$$

where v is the modelled variable such as wind speed or load, $C(\theta)$ is the normalising constant, θ_n are coefficients of B-splines, and $B_n(v)$ are B-splines.

3.3. Power system variables spatial correlation

The Kendall's tau correlation coefficient is used to assess whether the modelled load and wind speed preserves the spatial correlation of the measured load and wind speed data. The Kendall's tau correlation coefficient of two variables is given by equation (3.12) [51, 52, 67]. The correlation coefficient should be used only when data from two data sets X and Y has unique pairs in the form (x_1, y_1), (x_2, y_2) up to (x_n, y_n). The data sets are correlated if both $x_i > x_j$ and $y_i > y_j$ or both $x_i < x_j$ and $y_i < y_j$ [51, 52, 67]. Otherwise, the data sets are uncorrelated if $x_i > x_j$ while $y_i < y_j$ or if $x_i < x_j$ while $y_i > y_j$ [51, 52, 67].

$$\tau = \frac{2}{n(n-1)} \sum_{i=1}^{n} \sum_{i<j} sgn\big[(x_i - x_j)(y_i - y_j)\big] \tag{3.12}$$

where n is the sample size, sgn is the sign function, x_i and x_j are observations from the data set X, and y_i and y_j are observations from the data set Y.

3.4. Data range

Load and wind speed samples from the fitted distribution functions are sampled using Latin hypercube sampling (LHS) [68, 69]. The samples are used to test whether the distribution functions model the data range. LHS subdivides the sample space into equal intervals using the required sample size, and randomly samples from each interval [68, 69]. LHS samples probabilities from the sample space. Quantile functions (QFs) of the fitted distribution functions are then used to convert the sampled probabilities to synthetic load and wind speed values. The low and high measured and synthesised load and wind

speed values are then compared to determine whether the fitted distribution functions model the data range.

3.5. Wind turbine power curve

The Enercon E-82 E2, 2.05 MW wind turbine power curve [70] is used to convert wind speed to the power produced by the WPGs. Equation (3.13) is the piecewise mathematical model used to represent the Enercon wind turbine power curve. A two-parameter Weibull cumulative distribution function (CDF) given in equation (3.14) is used to model the wind turbine power curve [71]. The total power produced by a WPG with several wind turbines is given by equation (3.15) [72].

$$P_{WG} = \begin{Bmatrix} P(v) & 0 \leq v < v_{co} \\ 0 & v \geq v_{co} \end{Bmatrix} \tag{3.13}$$

$$P(v) = P_r\left(1 - e^{-\left(\frac{v}{\beta}\right)^{\delta}}\right) \tag{3.14}$$

$$P_{WPG} = \sum_1^n P_{WG_n} \tag{3.15}$$

where v_{co} is the wind turbine cut-out wind speed, v is the wind speed, δ and β are the Weibull CDF's shape and scale parameters, respectively, P_{WG_n} is the power produced by the nth wind turbine in a WPG, n is the number of wind turbines in a WPG, and P_r is the wind turbine's rated power.

3.6. Probabilistic transient stability assessment

3.6.1. Transient stability assessment

In a power system, synchronous generator (SG) rotor angular accelerations are defined by the swing equation shown in equation (3.16) [14, 73]. Based on the swing equation, the rotor of a SG does not accelerate if the generator's mechanical torque and the power system's electromagnetic toque at its terminals are balanced. Should the SG's mechanical torque become greater than the power system's electromagnetic torque, then the generator's rotor accelerates, however, this could result in transient instability

if the machine has a loss of synchronism with the power system. Similarly, if the SG's mechanical torque becomes less than the power system's electromagnetic torque, then the generator's rotor decelerates.

$$\frac{d^2\delta}{dt^2} = \frac{\omega}{2H}(P_m - P_e) \tag{3.16}$$

where δ is the rotor angle, ω is the rotor's angular velocity, H is the SG's inertia constant, P_m is the SG's mechanical torque, and P_e is the power system's electromagnetic torque at the SG's terminals.

3.6.2. Load and wind power generation sample size

The power system's probabilistic transient stability is assessed in this study using samples of load and power produced by WPGs. The samples are randomly sampled using Monte-Carlo Simulations (MCS). The required sample size for the load and the WPG's power production is quantified using the law of large numbers given by equation (3.17) [74]. The law of large numbers indicates that as the number of samples taken from a population is increased, the samples' mean approaches the population's mean [12]. The sample size becomes representative of the population when the sample mean stabilises.

$$\bar{X} = \lim_{n\to\infty} \sum_{i=1}^{n} \frac{X_i}{n} \tag{3.17}$$

where $\bar{X}$ is the population mean, X_i is the ith sampled value, and n is the number of samples taken.

3.6.3. Wind power generation penetration level

The wind power generation penetration level in the power system is quantified using equation (3.18) [75, 76]. Supplying a larger proportion of the load using WPGs increases their penetration level. As the wind power generation penetration level increases, the system net-load given by equation (3.19) is the portion of load that has to be supplied by SGs in the power system.

$$Penetration\ Level = \frac{\sum P_{WG}}{\sum P_L} \quad (3.18)$$

$$System\ Net - Load = \sum P_L - \sum P_{WG} \quad (3.19)$$

where P_{WG} is the power produced by WPGs, and P_L is the total system load.

3.7. Goodness of fit

The distribution functions' fit to the measured load and wind speed density is assessed using the root mean square error ($RMSE$) and the mean absolute error (MAE). Also, the similarity between the power system's transient stability results produced using modelled and measured load and wind speed is assessed using the $RMSE$ and MAE. The $RMSE$ given in equation (3.20) quantifies the square root of the squared mean error between two variables [41, 77], while the MAE given in equation (3.21) quantifies the mean of the absolute error between two variables [41, 77].

$$RMSE = \sqrt{\frac{1}{N}\sum_{i=1}^{N}\left(\hat{F}_i - F_i\right)^2} \quad (3.20)$$

$$MAE = \frac{1}{N}\sum_{i=1}^{N}\left|\hat{F}_i - F_i\right| \quad (3.21)$$

where $\hat{F}_i$ and F_i are probabilities of the i^{th} independent and dependent variable, and N is the number of samples.

3.8. Summary

The research process used in this study was presented in this chapter, and the research methods used were discussed. The research process considers the variability of the load and power produced by WPGs when assessing power system transient stability. The research process entails modelling the power system load and wind speed variability using distribution functions. The wind speed is then converted to the variable power produced by the WPGs. The impact of the variable load and power produced by the WPGs is assessed using the probabilistic method.

CHAPTER 4: POWER SYSTEM MODELLING

4.1. Introduction

The research methodology was presented in the previous chapter. This chapter discusses the power system and wind power generator (WPG) models used in this research. The power system equipment modelling discussed is load modelling, line modelling, transformer modelling, synchronous generator (SG) modelling, and WPG modelling. First, the IEEE 9-bus test system used as a case study in this research is introduced. Second, the modelling of the test system's components is discussed. Last, the WPG model and the integration of the WPGs to the test system are discussed.

4.2. Power system case study

Figure 4.1 shows the IEEE 9-bus test system single line diagram [78]. The test system is used as a case study. Gen 1 is operated as the reference machine, and it controls the balance between the load and power produced by the generators in the test system. Gen 2 is operated in synchronous condenser operation (SCO) mode to ensure that during periods of high wind power generation and low loading, the reference machine does not absorb active power because of excess generation. Furthermore, when operating in SCO mode, Gen 2 assists with the regulation of voltages in the test system. The test system load is located at buses 5, 6 and 8. Also, three WPGs are integrated at buses 5, 6 and 8.

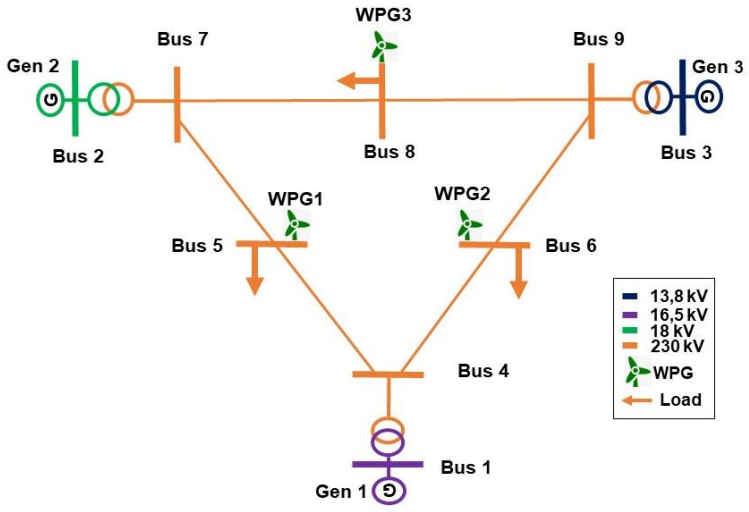

Figure 4.1: IEEE 9-bus test system single line diagram

4.3. Load modelling

The IEEE 9-bus test system load's active and reactive power components are modelled as constant power loads. The load's active and reactive power components are modelled using the polynomial load model shown below in equations (4.1) and (4.2), respectively [14]. The polynomial load model can model a constant impedance (Z), constant current (I), and constant power (P) load. To model a constant power load, the polynomial load model's active power coefficients p_1 and p_2 are set to 0 and p_3 is set to 1. Also, the polynomial load model's reactive power coefficients q_1 and q_2 are set to 0 and q_3 is set to 1.

$$P = P_o\,[p_1\,\tilde{\mathrm{V}}^2 + p_2\tilde{\mathrm{V}} + p_3\,] \tag{4.1}$$

$$Q = Q_o\,[q_1\,\tilde{\mathrm{V}}^2 + q_2\tilde{\mathrm{V}} + q_3\,] \tag{4.2}$$

where P_o and Q_o are the load's constant active and reactive power, p_1 , p_2 and p_3 are the active power coefficients, q_1 , q_2 and q_3 are the reactive power coefficients, and $\tilde{\mathrm{V}}$ is the load's voltage dependency factor given by the load's bus voltage divided by the nominal load bus voltage.

4.4. Line modelling

The IEEE 9-bus test system's power lines are modelled using the π model shown in Figure 4.2 [14, 79]. The line's inductive reactance (X_L) absorbs reactive power, while the line's susceptance (B) generates reactive power. The line's resistance (R_L) causes heat losses when current flows.

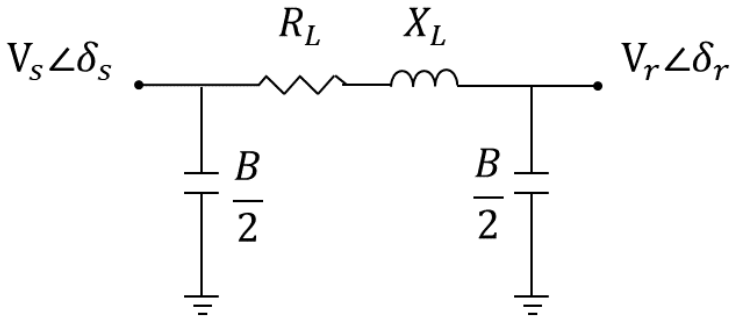

Figure 4.2: π model of a line

The line's inductive reactance and susceptance are given below in equations (4.3) and (4.4), respectively.

$$X_L = 2\pi f L \tag{4.3}$$

$$B = 2\pi f C = \frac{1}{X_C} \tag{4.4}$$

where L is the line's inductance, X_L is the line's inductive reactance, f is the power system frequency, B is the line's susceptance, X_C is the line's capacitive reactance, and C is the line's capacitance.

The reactive power absorbed or generated by the line's inductive reactance and susceptance is given below by equations (4.5) and (4.6), respectively.

$$Q_L = I^2 X_L \tag{4.5}$$

$$Q_C = V^2 B = \frac{V^2}{X_C} \tag{4.6}$$

where X_L and X_C are the line's inductive reactance and capacitive reactance, respectively, B is the line's susceptance, I is the current flowing across the line, and V is the line's bus voltage.

4.5. Transformer modelling

The IEEE 9-bus test system transformers are modelled as two-winding transformers shown in Figure 4.3 [14, 80]. The magnetising reactance (X_{ml}) models the transformer's saturation [14].

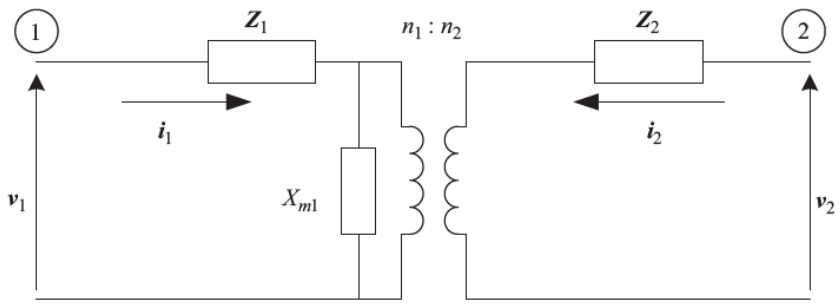

Figure 4.3: Model of a two-winding transformer

The transformer's impedance at each winding is given below in equation (4.7) [14, 80].

$$Z_i = R_i + jX_i \tag{4.7}$$

where R_i and X_i are the resistance and inductive reactance, respectively, of the transformer's primary winding (i.e., $i = 1$) or secondary winding (i.e. $i = 2$).

The winding ratio given below in equation (4.8) [14, 80] transfers the transformer's parameters from the primary winding to the secondary winding, and vice versa.

$$a = \frac{n_1}{n_2} \tag{4.8}$$

where n_1 and n_2 are the transformer's primary and secondary side number of windings.

The voltage at the transformer's primary (v_1) and secondary (v_2) side terminals is given below in equations (4.19) and (4.10), respectively [14, 80].

$$v_1 = Z_1 i_1 + a v_2 - a Z_2 i_2 \tag{4.9}$$

$$v_2 = Z_2 i_2 + \frac{1}{a} v_1 - \frac{1}{a} Z_1 i_1 \tag{4.10}$$

where Z_1 and Z_2 are the transformer's primary and secondary side impedances, respectively, i_1 and i_2 are the transformer's primary and secondary side currents, respectively, and a is the transformer's winding ratio.

4.6. Synchronous generator modelling

4.6.1. Synchronous generator mathematical modelling

The IEEE 9-bus test system is operated at a nominal frequency of 50 Hz. The SGs' synchronous speed (n) is given by equation (4.11) below [14]. The dynamic operation of the SGs is modelled using the GENROU dynamic model, which models the dynamic operation of round-rotor SGs. The parameters of the GENROU models for each of the IEEE 9-bus test system's SGs are given in Appendix A.

$$n = \frac{120f}{p} \tag{4.11}$$

where n is the SGs' synchronous speed, f is the power system frequency , and p is the SGs' number of poles.

The SGs are modelled in the d-q axis using Park's transformation to convert the machines' equations from the abc coordinate system to a d-q coordinate system [14, 81]. This is done to eliminate inductance variables in the formulation when the machines are modelled in the abc axis [14]. Based on the d-q coordinate system, the d-axis consists of the damper winding and excitation winding, while the q-axis consists of the 1q and 2q damper windings, as shown in Figures 4.4 and 4.5, respectively [81, 82].

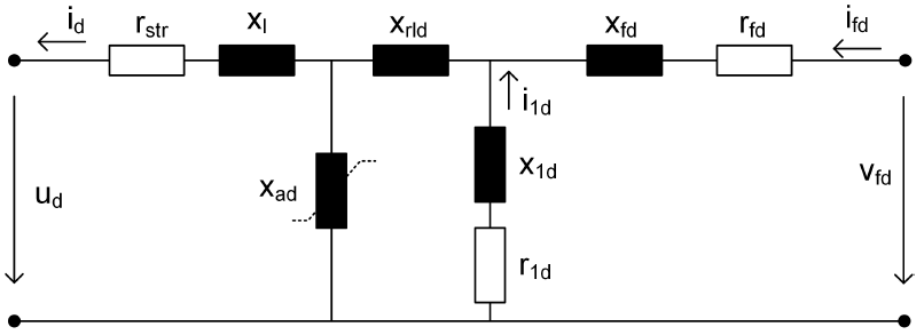

Figure 4.4: d-axis circuit of a round-rotor synchronous generator

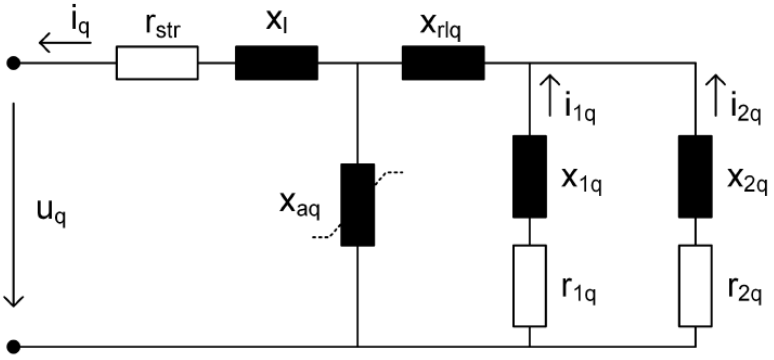

Figure 4.5: q-axis circuit of a round-rotor synchronous generator

During power system faults, the SGs' dynamic behaviour is a result of the transient behaviour of the stator and rotor. The SGs' per-unit stator voltages in the d-q axis are described below in equations (4.12) to (4.14) [14, 81, 82].

$$u_d = -r_{str} i_d - n\psi_q + \frac{1}{\omega_n}\frac{d\psi_d}{dt} \quad (4.12)$$

$$u_q = -r_{str} i_q + n\psi_d + \frac{1}{\omega_n}\frac{d\psi_q}{dt} \quad (4.13)$$

$$u_o = -r_{str} i_o + \frac{1}{\omega_n}\frac{d\psi_o}{dt} \quad (4.14)$$

where u_d and u_q are the d-axis and q-axis stator voltages, respectively, u_o is the zero-sequence voltage, i_d and i_q are the d-axis and q-axis stator currents, respectively, i_o is the zero-sequence current, ψ_d and ψ_q are the d-axis and q-axis stator flux linkages, respectively, ψ_o is the zero sequence stator flux linkage, n is the rotor's synchronous speed, ω_n is the rotor's operating speed, and r_{str} is the stator resistance.

The SGs' rotor voltages in the d-axis are described below by equations (4.15) and (4.16) [14, 81, 82].

$$v_{fd} = r_{fd} i_{fd} + \frac{1}{\omega_n}\frac{d\psi_{fd}}{dt} \quad (4.15)$$

$$0 = r_{1d} i_{1d} + \frac{1}{\omega_n}\frac{d\psi_{1d}}{dt} \quad (4.16)$$

where v_{fd} is the d-axis field voltage, r_{fd} is the d-axis field winding resistance, r_{1d} is the d-axis 1d damper resistance, i_{fd} is the d-axis field winding current, ψ_{fd} is the d-axis field winding flux linkage, ψ_{1d} is the d-axis 1d damper flux linkage, and ω_n is the rotor's operating speed.

The SGs' rotor voltages in the q-axis are described below by equations (4.17) and (4.18) [14, 81, 82].

$$0 = r_{1q} i_{1q} + \frac{1}{\omega_n}\frac{d\psi_{1q}}{dt} \quad (4.17)$$

$$0 = r_{2q} i_{2q} + \frac{1}{\omega_n}\frac{d\psi_{2q}}{dt} \quad (4.18)$$

where r_{1q} and r_{2q} are the q-axis 1q damper and 2q damper resistances, i_{1q} and i_{2q} are the q-axis 1q damper and 2q damper currents, ψ_{1q} and ψ_{2q} are the q-axis 1q damper and 2q damper flux linkages, and ω_n is the rotor's operating speed.

4.6.2. Excitation system

The IEEE 9-bus test system's SGs are equipped with the IEEET1 excitation system to regulate their terminal voltages at the setpoints shown in Table 4.1. The parameters of the SGs' IEEET1 excitation systems are given in Appendix A. The SGs' terminal voltages are kept constant at the setpoints to regulate the voltages in the test system [14]. The SGs' terminal voltages are maintained at the setpoints by the excitation systems which control the field current, that in turn controls the machine's field voltage [14, 83].

Table 4.1: Synchronous generator voltage setpoints

Generator	Voltage Setpoint (pu)
Gen 1	1.040
Gen 2	1.025
Gen 3	1.025

4.6.3. Governor system

The IEEE 9-bus test system SGs are equipped with BPA_GG governor system dynamic model. The governor system parameters for each of the SGs are given in Appendix A. The power produced by the SGs is regulated by controlling the generators mechanical torque [83], which in turn is controlled by regulating the steam driving the turbines [83]. The governor system measures the turbine's speed and determines whether it is less or greater than the required speed. The feedback from the governor system is used to adjust the steam driving the turbine [83].

4.7. Wind power generator modelling

4.7.1. Wind power generator system

The WPGs integrated into the IEEE 9-bus test system are modelled using the IEC 61400-27-1 Type 4B generic WPG model, whose structure is shown in Figure 4.6 [84]. The model consists of five systems, namely, the control system, the generator system, the grid protection system, the electrical equipment, and the mechanical system. The control system models the WPGs' reactive power control (Q control), current limitation, reactive power limitation (Q limitation), and power control (P control). The generator

system models the dynamics of the generator, while the grid protection system controls the conditions under which during power system disturbances, the WPGs should not disconnect from the grid. The electrical equipment consists of the WPGs' buses, transformers, and circuit breakers, while the mechanical system models the interactions between the turbine and the generator.

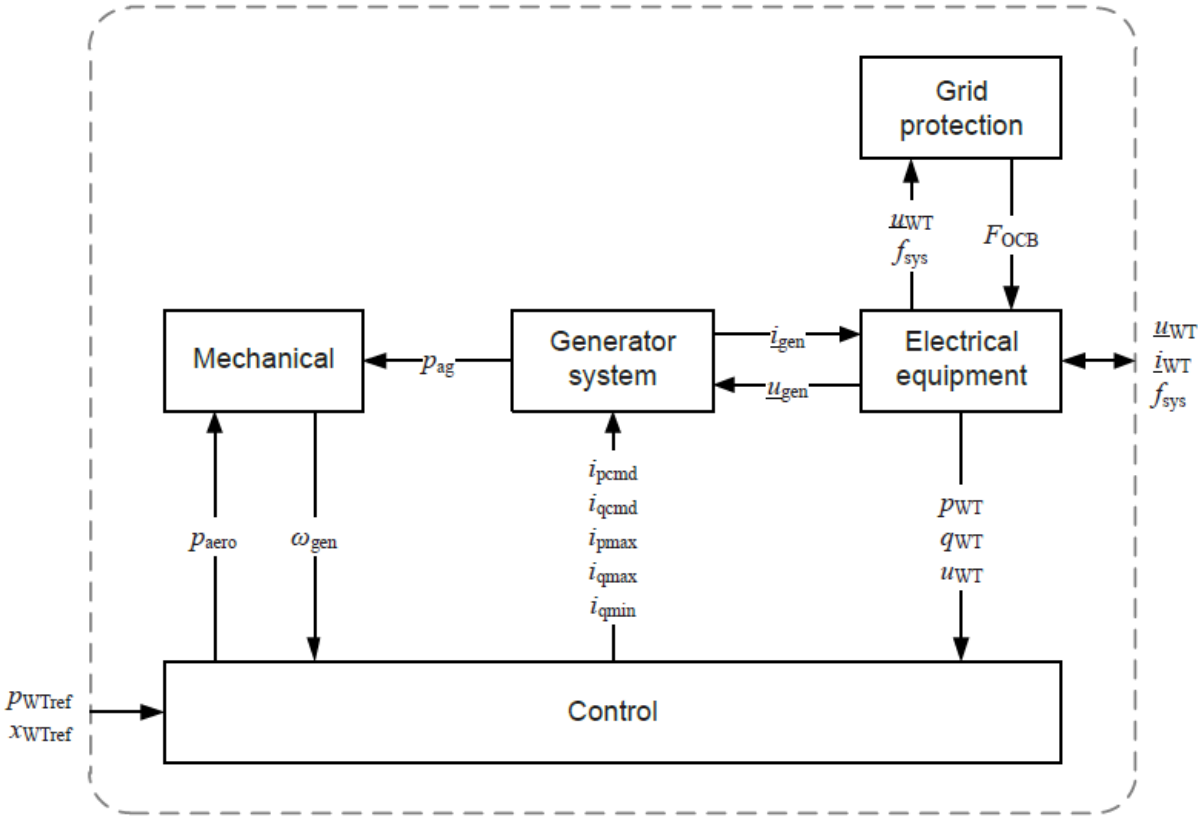

Figure 4.6: Type 4B wind power generator model

4.7.2. Mechanical model

The turbine and generator are modelled as a two-mass system shown in Figure 4.7 [84]. A spring and damper system models the interactions between the two masses. The two-mass system accounts for oscillations between the turbine and the generator during power system disturbances.

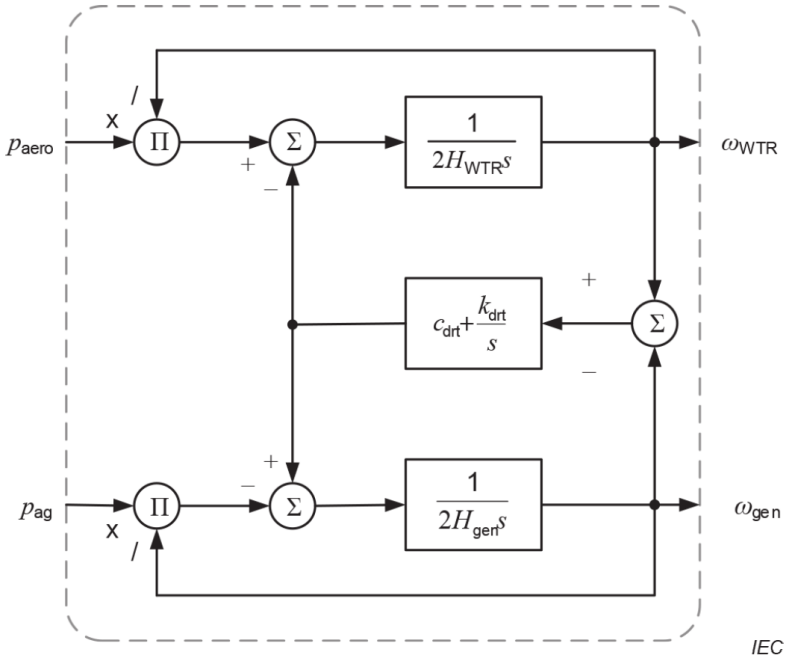

Figure 4.7: Wind power generator mechanical model

4.7.3. Generator system

The generator is integrated into the power system via a fully-rated converter [84]. As a result, the generator's dynamics are decoupled from the power system. The parameters of the generator are shown in Table 4.2.

Table 4.2: Generator parameters

Parameters	Symbol	Values
Time constant (s)	T_g	0.01
Reactive minimum current ramp rate (I_{base}/s)	di_{qmin}	-100
Active current maximum ramp rate (I_{base}/s)	di_{pmax}	1
Reactive current maximum ramp rate (I_{base}/s)	di_{qmax}	100

4.7.4. Electrical equipment

The WPGs' electrical equipment consists of 0.69/20kV collector system step-up transformers. The collector system step-up transformers step-up the power produced by the wind turbines. There is a 20/132kV grid integration step-up transformer that integrates the WPGs to the 132kV distribution network. Also, the electrical equipment consists of 0.69kV, 20kV, and 132kV buses and circuit breakers.

4.7.5. Grid protection model

The WPGs' grid protection model is configured so that the plant has voltage ride-through characteristics stipulated in the South African grid connection code for renewable power plants (RSA RPP Grid Code) [85]. The RSA RPP Grid Code's voltage ride-through requirement for inverter-based generators is shown in Figure 4.8 [85]. Based on the voltage ride-through requirements, the WPGs should remain synchronised to the test system for as long as the voltages at their point of connection (POC) remain within areas A, B, and D [85, 86].

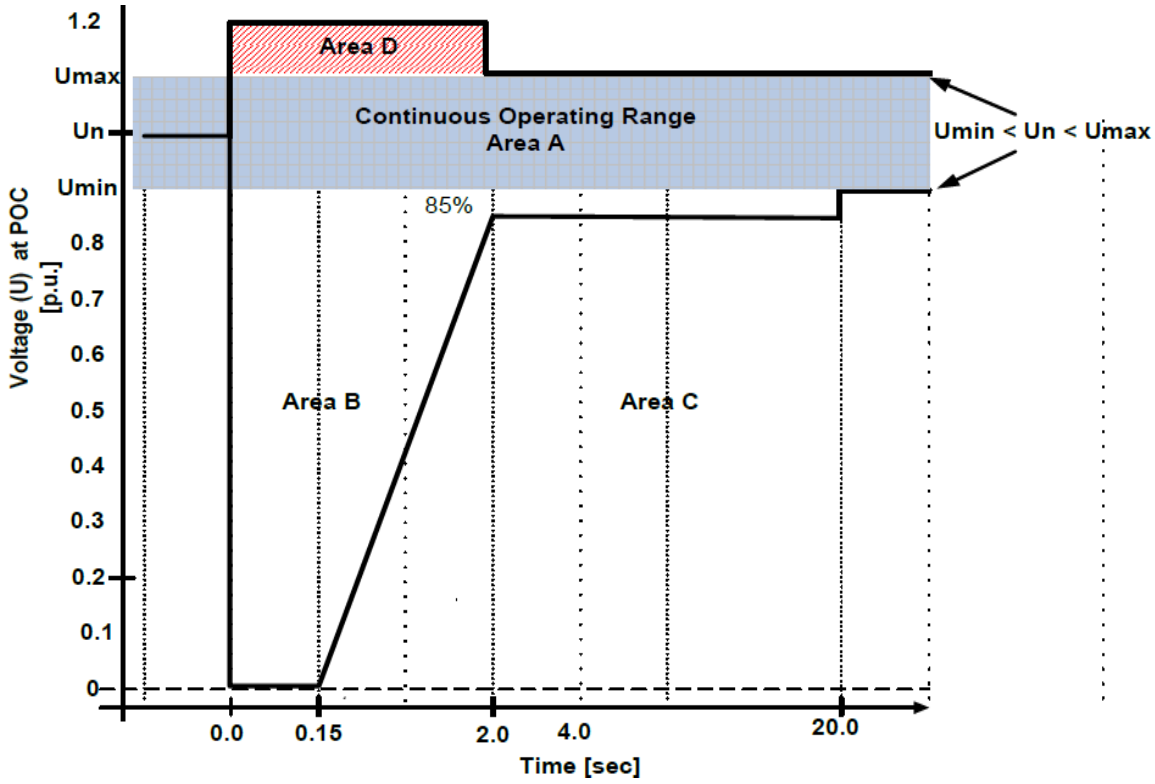

Figure 4.8: Inverter-based generator voltage ride-through capability

4.7.6. Control models

The control of the wind turbines is performed by different controllers. The controllers used in the model are a P-controller, a Q-controller, a Q-limitation controller, and a current-limitation controller [84]. The four controllers are integrated as shown in Figure 4.9 [84].

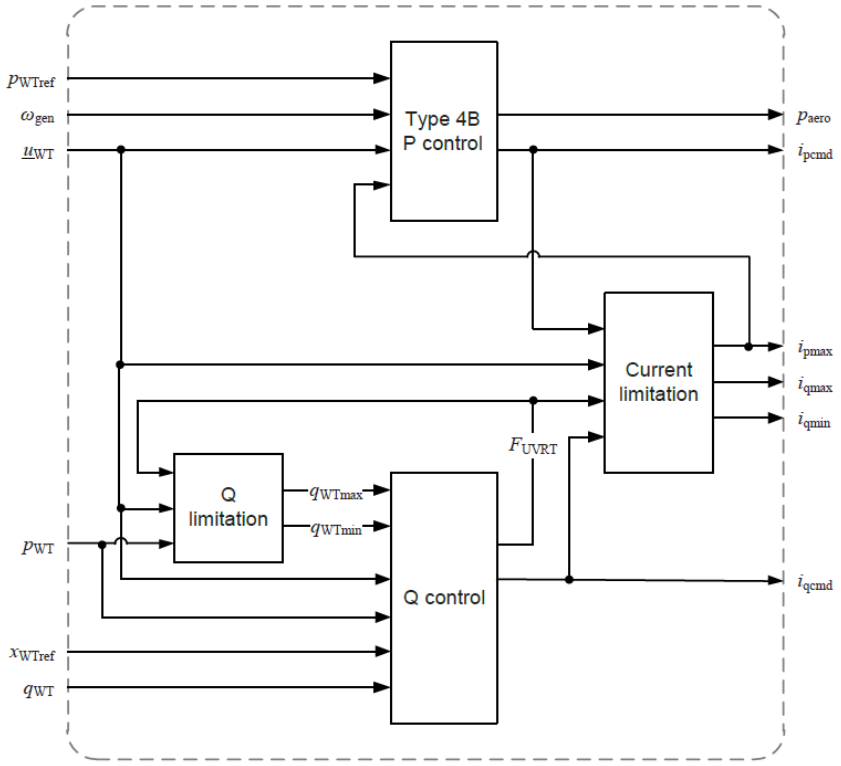

Figure 4.9: Type 4B wind turbine control model structure

The wind turbines' active power production is managed by the P-controller [87], which reduces the error between the wind turbines' reference rotational speed and their measured rotational speed [87]. The signals produced by the P-controller are fed to the wind turbines and the current-limitation controller. The wind turbines' reactive power production is managed by the Q-controller. The wind turbines can operate in power factor control, voltage control, reactive power control, open-loop reactive power control, and open-loop reactive power factor control modes [84]. In this research, the wind turbines are operated in voltage control mode, with a 1.03 pu voltage setpoint. The Q-limitation controller manages the wind turbines' low and high reactive power limits [84]. The reactive power limits from the Q-limitation controller are fed into the Q-controller. The current limitation controller combines the wind turbines' limits with the other controller limits, and produces active and reactive power current limits [84, 87]. The signals produced by the current-limitation controller are fed to the wind turbines and the P-controller.

4.7.7. Wind power generator integration

Figure 4.10 shows the WPG models and their integration to the IEEE 9-bus test system. Each WPG has a capacity of 10.25 MW, and is modelled by aggregating five 2.05 MW fully-rated converter wind turbines. The WPGs are integrated into the test system at buses 5, 6, and 8 using 132/230kV transformers. Each WPG integrates to the 132/230kV transformers using a single circuit, 40km, 132kV Wolf line, templated at 50º Celsius.

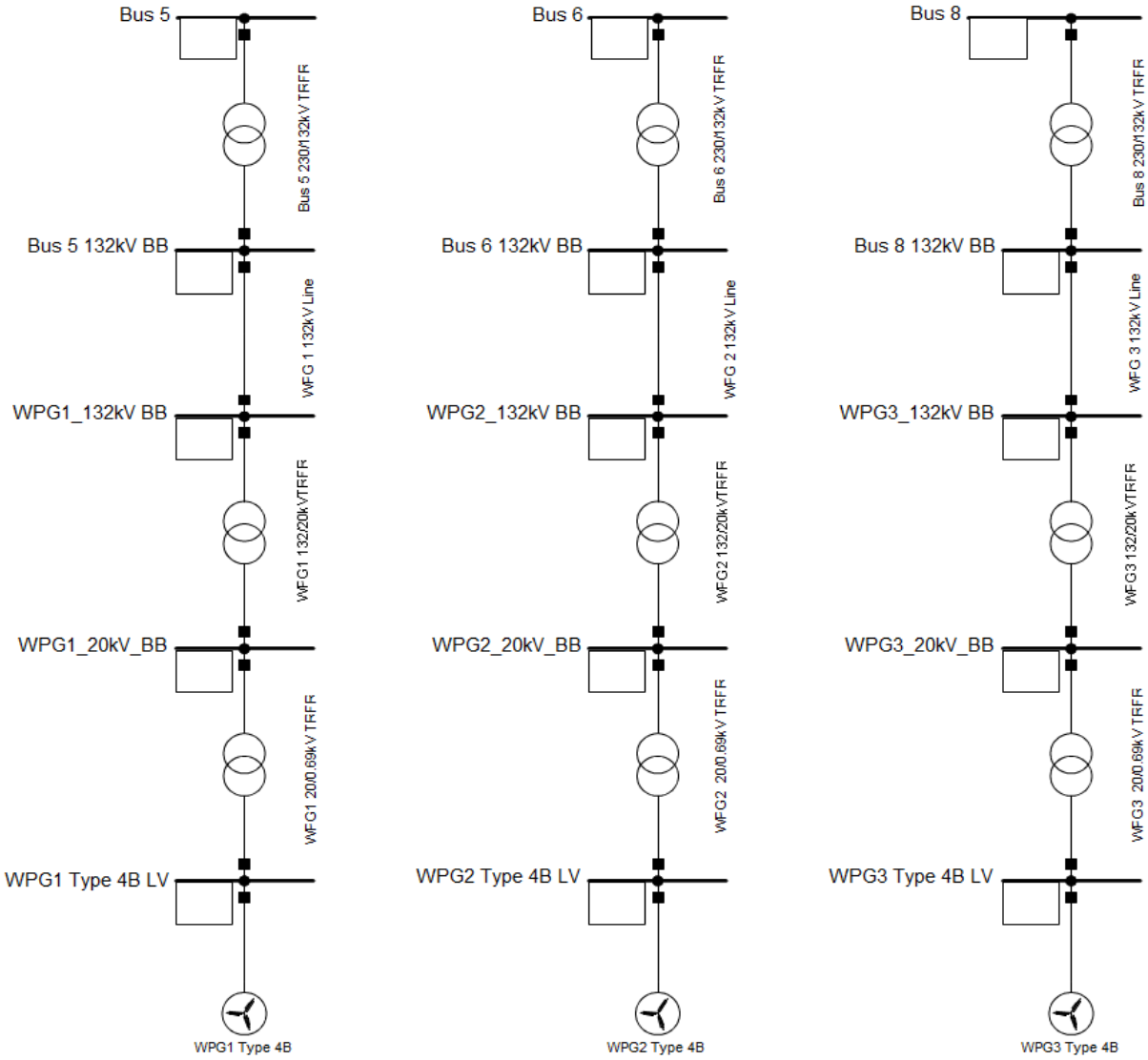

Figure 4.10: Wind power generator diagram

4.8. Summary

In this chapter, the IEEE 9-bus test system and the WPG models used in this research were discussed. The test system loads are modelled as constant power loads. The GENROU dynamic model is used to model the SGs dynamic performance. The SGs excitation systems are modelled using the IEEET1 excitation system dynamic model. Furthermore, the SGs are equipped with the BPA_GG governor system dynamic model. The WPGs are modelled using the IEC 61400-27-1 Type 4B generic WPG model. The WPGs' generic model consists of a control system, a generator system, a grid protection system, electrical equipment, and a mechanical system. The WPGs are operated in voltage control mode, with a 1.03 pu voltage setpoint.

CHAPTER 5: LOAD VARIABILITY MODELLING

5.1. Introduction

In the previous chapter, the modelling of the IEEE 9-bus test system and the wind power generators (WPGs) was discussed. In this chapter, measured load is assigned to each of the three IEEE 9-bus test system load buses to model power system variability. The load is then modelled using seven distribution functions consisting of the parametric Gaussian, Rayleigh, Wakeby, Gaussian mixture model (GMM) and Kappa, and the non-parametric Kernel density estimation (KDE) and Logspline density estimation (LDE). Then, the impact of the modelled load on the transient stability of the test system is investigated.

5.2. Power system load variability modelling

5.2.1. Measured load data

Substation loading data from three South African substations supplying residential load is used in this study. The load was measured in five-minute intervals from 1 January 2019 to 31 December 2019. The substation load is assigned to the IEEE 9-bus test system load buses. Peak load demand at each of the test system load buses is used to normalise the assigned load. Table 5.1 shows the range of the test system load at each load bus.

Table 5.1: IEEE 9-bus test system load range

Load Range	Load Bus 5 (MW)	Load Bus 6 (MW)	Load Bus 8 (MW)
High	125.000	90.000	100.000
Low	31.604	27.640	14.366

5.2.2. Load modelling using distribution functions

The load is modelled using the parametric Rayleigh, Gaussian, Wakeby, GMM, Kappa and the non-parametric LDE and KDE. The fitted Rayleigh, Gaussian, Wakeby, and Kappa parameters are shown in Tables 5.2 to 5.5, respectively, while Tables 5.6 to 5.8 show the fitted GMM's weight, mean, and standard deviation parameters, respectively.

Table 5.2: Rayleigh parameters

Load Bus	Location	Scale
Load Bus 5	31.983	26.506
Load Bus 6	36.640	16.317
Load Bus 8	11.079	23.273

Table 5.3: Gaussian parameters

Load Bus	Mean	Standard Deviation
Load Bus 5	65.204	17.246
Load Bus 6	57.091	10.617
Load Bus 8	40.247	15.142

Table 5.4: Wakeby parameters

Load Bus	Location	Scale 1	Scale 2	Shape 1	Shape 2
Load Bus 5	35.731	62.955	1.268	0.664	0.613
Load Bus 6	34.966	73.354	5.394	14.914	-0.400
Load Bus 8	9.044	462.876	32.365	19.568	-0.129

Table 5.5: Kappa parameters

Load Bus	Location	Scale	Shape 1	Shape 2
Load Bus 5	51.782	27.165	0.499	0.505
Load Bus 6	52.773	11.587	0.341	0.098
Load Bus 8	30.877	13.190	-0.017	0.244

Table 5.6: GMM's weight parameters

Load Bus	Weight 1	Weight 2	Weight 3
Load Bus 5	0.249	0.678	0.073
Load Bus 6	0.336	0.441	0.223
Load Bus 8	0.091	0.571	0.338

Table 5.7: GMM's mean parameters

Load Bus	Mean 1	Mean 2	Mean 3
Load Bus 5	44.544	70.002	91.089
Load Bus 6	46.095	58.896	70.053
Load Bus 8	20.480	33.864	56.386

Table 5.8: GMM's standard deviation parameters

Load Bus	Standard Deviation 1	Standard Deviation 2	Standard Deviation 3
Load Bus 5	5.303	12.202	12.993
Load Bus 6	6.004	5.056	5.800
Load Bus 8	1.336	6.240	15.621

Figure 5.1 shows the density plots of the three IEEE 9-bus test system load buses that are modelled using the Gaussian, Rayleigh, Wakeby, Kappa, GMM, KDE, and LDE. Load bus 5 had a bimodal load density because it had two peaks. The Gaussian, Rayleigh, Wakeby, and Kappa do not model load bus 5's bimodal load density because

they only model densities with a single peak. However, the GMM, KDE, and LDE model load bus 5's bimodal load density. The GMM models load bus 5's bimodal load density because the three Gaussian distribution functions that it fitted can model densities with two peaks. Also, the KDE and LDE model load bus 5's bimodal load density because they use Gaussian kernels and basis-splines (B-splines), respectively, which can fit bimodal densities. The load density at load buses 6 and 8 has a single peak, and the seven distribution functions assessed can model unimodal densities.

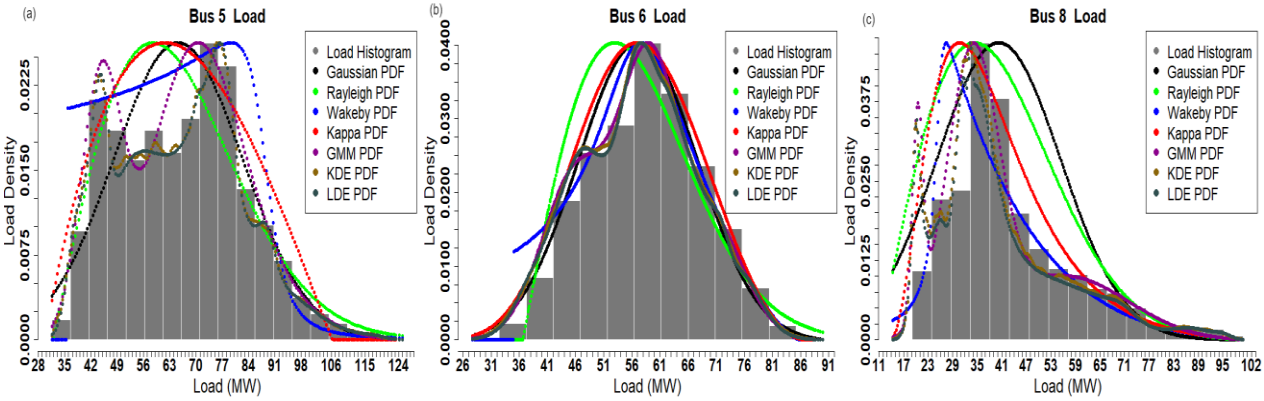

Figure 5.1: PDF modelled load: (a) bus 5 load, (b) bus 6 load, (c) bus 8 load

5.2.3. Load spatial correlation

Table 5.9 shows the spatial correlation of the three loads in the IEEE 9-bus test system. The load's spatial correlation is evaluated using the Kendall's tau correlation coefficient. The assessment is performed to determine whether the modelled load maintains the measured load's spatial correlation. The spatial correlation between the measured load at buses 5 and 6, buses 5 and 8, and buses 6 and 8 is similar to the spatial correlation of the load that was modelled when using the seven distribution functions at the same buses. These results show that the modelled load preserves the measured load's spatial correlation.

Table 5.9: Load spatial correlation

Load	Load Buses 5 and 6	Load Buses 5 and 8	Load Buses 6 and 8
Measured Load	0.418950	0.499111	0.317247
Gaussian Load	0.418930	0.499083	0.317221
Rayleigh Load	0.418930	0.499083	0.317221
Wakeby Load	0.418946	0.499101	0.317241
Kappa Load	0.418944	0.499101	0.317239
GMM Load	0.418930	0.499083	0.317221
KDE Load	0.418950	0.499111	0.317247
LDE Load	0.418930	0.499083	0.317221

5.2.4. Distribution functions fit to load

Figure 5.2 shows the IEEE 9-bus test system's measured load empirical cumulative distribution functions (ECDFs). Figure 5.2 also shows the cumulative distribution functions (CDFs) of the fitted Gaussian, Rayleigh, Wakeby, Kappa, GMM, KDE, and LDE. The shapes of the fitted distribution functions' CDFs are similar to the measured loads' ECDFs. However, compared with lower loads, at higher loads the fitted distribution functions' CDFs are closer to the measured loads' ECDFs. This indicates that the fitted distribution functions have a better fit to higher loads than to lower loads.

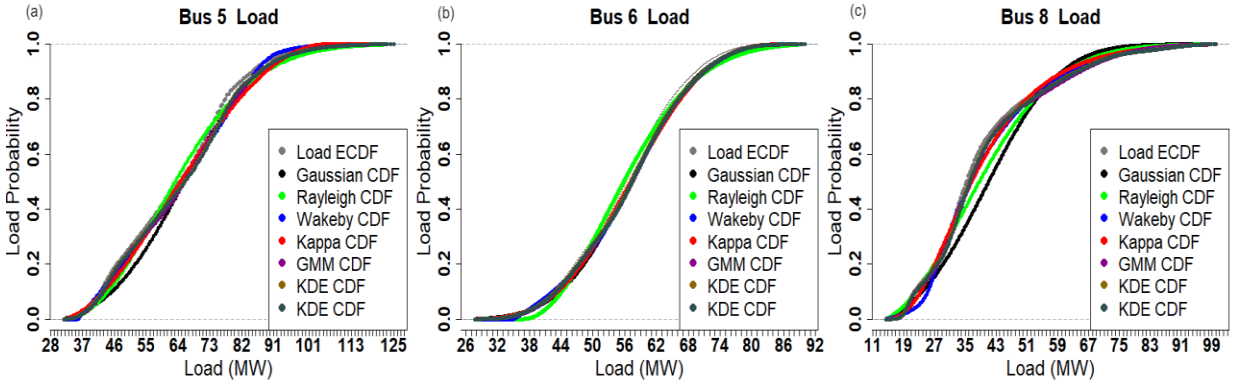

Figure 5.2: CDF modelled load: (a) bus 5 load, (b) bus 6 load, (c) bus 8 load

Tables 5.10 and 5.11 show the root mean square error (RMSE) and mean absolute error (MAE) of the fitted Gaussian, Rayleigh, Wakeby, Kappa, GMM, KDE and LDE CDFs. At the three IEEE 9-bus test system load buses, the KDE has the best fit to the load, followed by the LDE and then the GMM. The Wakeby has the fourth-best fit when modelling load at buses 5 and 6, followed by the Kappa, then the Gaussian, and last the Rayleigh. The Kappa has the fourth-best fit when modelling load at bus 8, followed by the Wakeby, then the Rayleigh, and last the Gaussian.

Table 5.10: RMSE of distribution functions fitted to the load

Load Bus	Gaussian	Rayleigh	Wakeby	Kappa	GMM	KDE	LDE
Load Bus 5	0.02746	0.03403	0.01417	0.02019	0.00907	0.00141	0.00473
Load Bus 6	0.00997	0.03167	0.00580	0.00850	0.00286	0.00228	0.00234
Load Bus 8	0.07020	0.04329	0.02465	0.02237	0.00621	0.00117	0.00413

Table 5.11: MAE of distribution functions fitted to the load

Load Bus	Gaussian	Rayleigh	Wakeby	Kappa	GMM	KDE	LDE
Load Bus 5	0.02190	0.02880	0.01093	0.01742	0.00750	0.00118	0.00429
Load Bus 6	0.00740	0.02644	0.00438	0.00710	0.00228	0.00201	0.00216
Load Bus 8	0.05541	0.03448	0.02013	0.01912	0.00530	0.00091	0.00347

5.2.5. Load range synthesis

Table 5.12 shows the load range synthesised by the fitted Gaussian, Rayleigh, Wakeby, Kappa, GMM, KDE, and LDE. The load range synthesised by the different distribution functions differ due to some of the distribution functions having longer lower and upper tails than others. The distribution functions' lower and upper tails determine the low and high load values, respectively, that can be synthesised. A comparison of the measured low and high load values in Table 5.1 with the synthesised low and high load values in Table 5.12 shows that some of the distribution functions do not synthesise the load range at the three test system load buses. The Gaussian synthesises the load range at load bus 6, while at load buses 5 and 8, it synthesises maximum load only. Also, at load buses 5 and 8, the Gaussian synthesises negative low load, while Table 5.1 shows that the measured low load is positive. The Rayleigh synthesises the load range at load bus 8, but at load buses 5 and 6, it synthesises maximum load only. The Wakeby synthesises the load range at load bus 8, however, at load bus 5, the Wakeby synthesises maximum load only, and does not synthesise both low and high loads at load bus 6. The Kappa synthesises the load range at load bus 8, while at load buses 5 and 6, the Kappa synthesises low load only. The GMM synthesises the load range at load buses 5 and 6, but at load bus 8, it synthesises maximum load only. Furthermore, at load bus 8, the GMM synthesises negative low load, while Table 5.1 shows that the low load should be positive. The KDE and the LDE synthesise the load range at the three load buses. The distribution functions' ability to synthesise the load range indicates that their lower and upper tails extend to the low and high load values at each load bus.

Table 5.12: Synthesised load range

Loads	Statistic	Gaussian	Rayleigh	Wakeby	Kappa	GMM	KDE	LDE
Load Bus 5	High (MW)	143.923	166.605	3020.107	106.125	142.809	125.025	128.183
	Low (MW)	-12.733	32.049	35.732	29.746	15.864	31.574	24.554
Load Bus 6	High (MW)	105.380	119.268	85.620	86.299	94.543	90.029	95.132
	Low (MW)	7.201	36.667	34.966	19.181	19.252	27.606	17.470
Load Bus 8	High (MW)	107.803	127.030	144.367	212.721	122.354	100.030	101.794
	Low (MW)	-26.757	11.151	9.047	13.147	-8.984	14.327	12.749

5.3. Load variability modelling impact on transient stability

5.3.1. Load sample size

Monte-Carlo Simulations are used to randomly sample 2000 load values from each of the measured and the modelled load data. Figures 5.3 to 5.5 show the moving means of the normalised sampled load of buses 5, 6, and 8, respectively. The required load sample size to perform the probabilistic transient stability studies is quantified based on the law of large numbers given by equation (3.17). The sample size is based on the number of samples required for the load's moving mean to stabilise. About 768 samples are required for buses 5 and 8 loads' moving mean to stabilise, and about 532 samples are required for bus 6 load's moving mean to stabilise. Therefore, at each load bus, a minimum of 768 load samples is required to ensure that the sampled load represents the measured load data. In this study, 1000 load samples are used to investigate power system transient stability using the probabilistic method.

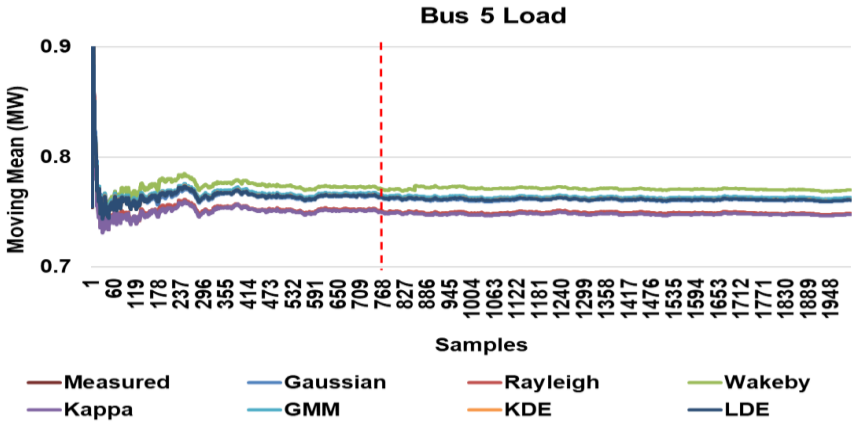

Figure 5.3: Bus 5 normalised load moving mean

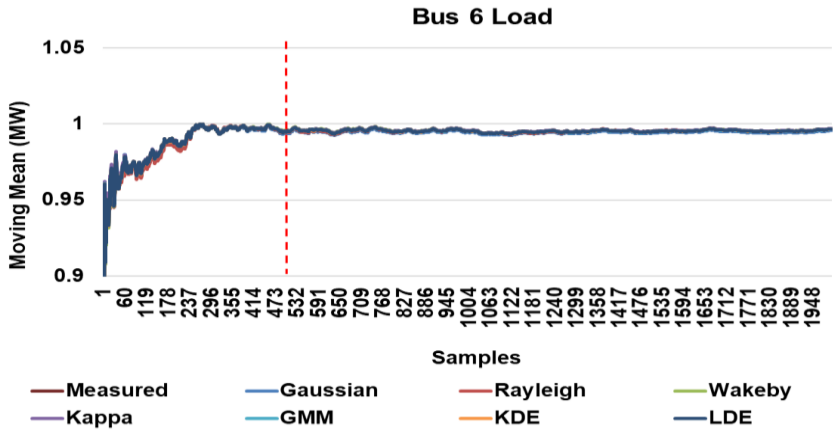

Figure 5.4: Bus 6 normalised load moving mean

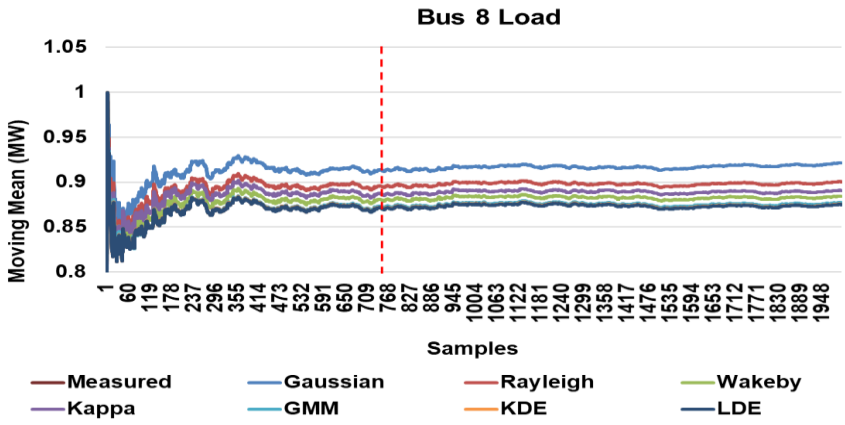

Figure 5.5: Bus 8 normalised load moving mean

5.3.2. Transient stability of power system with variable load

For each of the 1000 load samples taken for load buses 5, 6, and 8, studies are performed to determine the impact of load variability modelling on the IEEE 9-bus test system's transient stability. Figure 5.6 shows Gen 3's maximum rotor angle deviation ECDFs produced when the test system's load variability is modelled using measured and modelled load. When three-phase faults are applied sequentially on line 6-9 and line 8-9, close to bus 9, Gen 3's rotor angle deviation ECDFs produced when load variability is modelled using the KDE and LDE closely follow those produced when measured load is used. However, Gen 3's rotor angle deviation ECDFs produced when load modelled using the Gaussian, Rayleigh, Wakeby, Kappa, and GMM is used do not closely follow those produced when measured load is used. Modelling load using the Gaussian and GMM produces Gen 3's maximum rotor angle deviation ECDFs that are located above those produced when measured load is used. This indicates that modelling load variability using the Gaussian and GMM results in the power system operating with a lower risk of transient instability than when measured load is used. In Figure 5.6, it can also be seen that compared with when measured load is used, modelling load using the Gaussian and GMM results in a larger proportion of Gen 3's maximum rotor angle deviations being located within lower rotor angle deviation values, indicating better power system stability. However, modelling load using the Rayleigh, Wakeby, and Kappa produces Gen 3's maximum rotor angle deviation ECDFs located below those produced when measured load is used. This indicates that modelling load variability using the Rayleigh, Wakeby, and Kappa results in the power system operating with a

higher risk of transient instability than when measured load is used. Referring to Figure 5.6, it can also be seen that compared with when measured load is used, modelling load using the Rayleigh, Wakeby, and Kappa results in a larger proportion of Gen 3's maximum rotor angle deviations being located within higher rotor angle values, indicating worse power system stability.

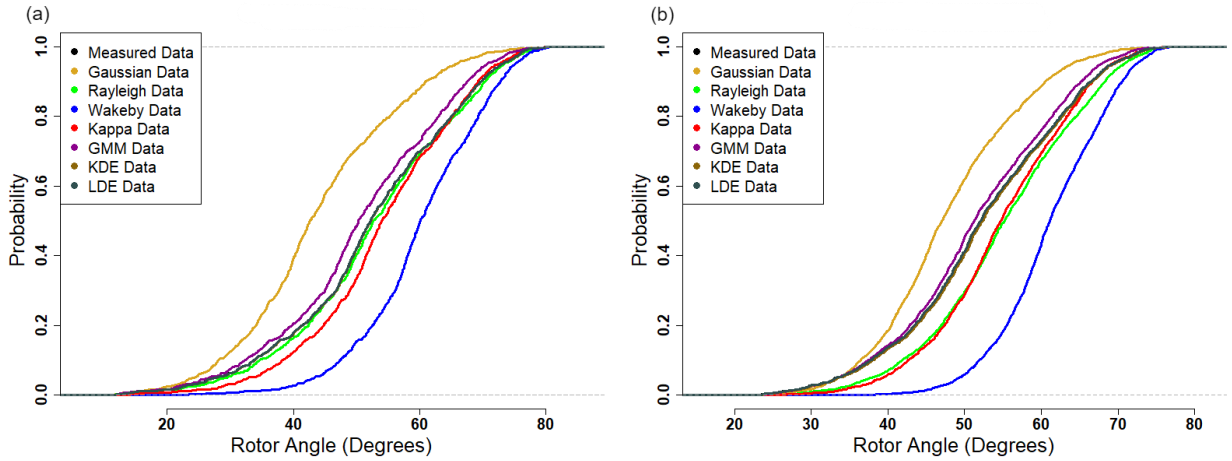

Figure 5.6: Gen 3 maximum rotor angle deviation ECDFs owing to load variability when faults were applied close to bus 9 on: (a) line 6-9, (b) line 8-9.

Tables 5.13 and 5.14 show the respective RMSE and MAE results that compare Gen 3's maximum rotor angle deviation ECDFs obtained when measured and modelled load is used. The results show that Gen 3's maximum rotor angle deviations obtained when load is modelled using the KDE, LDE, and GMM have the best, second-best, and third-best RMSE and MAE, respectively.

Table 5.13: Gen 3 maximum rotor angle deviation ECDFs RMSE owing to modelled load

Fault	Gaussian Data	Rayleigh Data	Wakeby Data	Kappa Data	GMM Data	KDE Data	LDE Data
Line 6-9	0.024701	0.021240	0.013894	0.012772	0.007134	0.001094	0.001182
Line 8-9	0.024482	0.021713	0.012737	0.012803	0.006232	0.000852	0.000915

Table 5.14: Gen 3 maximum rotor angle deviation ECDFs MAE owing to modelled load

Fault	Gaussian Data	Rayleigh Data	Wakeby Data	Kappa Data	GMM Data	KDE Data	LDE Data
Line 6-9	0.019452	0.016406	0.010640	0.009718	0.004534	0.000646	0.000742
Line 8-9	0.019085	0.016824	0.009858	0.009708	0.004128	0.000569	0.000607

5.4. Discussion of results

In section 5.2, the density of the IEEE 9-bus test system load is modelled using the Gaussian, Rayleigh, Wakeby, Kappa, GMM, KDE, and LDE. In Table 5.9, the results show that the load modelled by the distribution functions preserves the measured load's spatial correlation at the three test system load buses. Also, Tables 5.10 and 5.11 show that based on fit, the distribution functions that do not rely on parameters to determine their shape (i.e., KDE and LDE) fit the load density better than those that rely on parameters (i.e., Gaussian, Rayleigh, Wakeby, Kappa, and GMM). This is because distribution functions with parameters have defined shapes they can model, and so are limited in the shapes of load densities they model. In Table 5.12, when considering the distribution functions load range modelling ability, it is found that only the KDE and the LDE model the load range at the three test system load buses. These findings show that not all of the distribution functions can model the load range. As a result, it is important that when assessing the distribution functions' ability to model load density, in addition to their fit, they should also be assessed to determine whether they model the load range. Distribution functions' ability to model the load range ensures that they synthesise low and high power system loading conditions.

In section 5.3, the impact of load variability modelling on the IEEE 9-bus test system's transient stability is assessed. Tables 5.13 and 5.14 show that load modelled using distribution functions that do not have parameters (i.e., KDE and LDE) produces power system transient stability results similar to those produced when measured load is used. The power system transient stability results produced using load modelled by distribution functions whose shapes depend on parameters (i.e., Gaussian, Rayleigh, Wakeby, Kappa, and GMM) are less similar to those produced when measured load is used. This is because the KDE and the LDE fit the load density better than the Gaussian, Rayleigh, Wakeby, Kappa, and GMM. These findings show that the KDE and LDE are good candidates for modelling power system load variability.

5.5. Summary

In this chapter, seven distribution functions, namely, the Gaussian, Rayleigh, Wakeby, Kappa, GMM, KDE, and LDE were used to model the IEEE 9-bus test system's load variability. The distribution functions were assessed on the basis of their fit and their ability to synthesise the load range. Furthermore, the impact of the modelled load on the transient stability of the test system was investigated. It was found that of the seven distribution functions that were assessed, the KDE and the LDE had the best fit to load density at the test system load buses. It was also found that some of the distribution functions did not model the load range. Furthermore, it was found that load modelled using the KDE and the LDE resulted in the test system having transient stability results similar to those produced when measured load was used.

CHAPTER 6: WIND SPEED VARIABILITY MODELLING

6.1. Introduction

In the previous chapter, load variability from three South African substations supplying residential load was modelled using seven distribution functions. Furthermore, the impact of the variable load on the IEEE 9-bus test system's transient stability was assessed. In this chapter, wind speed is modelled using seven distribution functions consisting of the parametric Rayleigh, Weibull, Wakeby, Gumbel and Kappa, and the non-parametric Logspline density estimation (LDE) and Kernel density estimation (KDE). The variable power produced by wind power generators (WPGs) that are integrated to the IEEE 9-bus test system is developed using the wind speed. An investigation is then performed to assess the impact of the integrated WPGs on power system transient stability.

6.2. Wind speed modelling

6.2.1. Measured wind speed data

Five-minute interval wind speed, measured at a height of 10 m at three sites in South Africa from 1 January 2019 to 31 December 2019, is used in this study. To develop the power produced by WPGs with wind turbines that have a 100 m hub height, the wind speed is converted to a height of 100 m using the power exponent formula shown below in equation (6.1). Table 6.1 shows the measured wind speed range at a height of 100 m.

$$v_2 = v_1 \left(\frac{h_2}{h_1}\right)^{\alpha} \tag{6.1}$$

where v_1 is height h_1 wind speed, v_2 is height h_2 wind speed, and the wind speed shear exponent is α.

Table 6.1: Wind speed range

Wind Speed Range	Site 1 (m/s)	Site 2 (m/s)	Site 3 (m/s)
High	25.845	23.899	22.371
Low	0.556	0.417	0.417

6.2.2. Wind speed modelling using distribution functions

The parametric Gumbel, Weibull, Wakeby, Rayleigh, Kappa, and the non-parametric LDE and KDE are used to model the wind speed. The fitted Gumbel, Weibull, Wakeby, Rayleigh, and Kappa parameters are shown in Tables 6.2 to 6.6, respectively.

Table 6.2: Gumbel parameters

Site	Location	Scale
Site 1	3.601	2.617
Site 2	3.873	2.859
Site 3	2.987	2.041

Table 6.3: Weibull parameters

Site	Shape	Scale
Site 1	1.597	5.745
Site 2	1.837	7.096
Site 3	1.333	3.795

Table 6.4: Wakeby parameters

Site	Location	Scale 1	Scale 2	Shape 1	Shape 2
Site 1	0.501	6.199	17.201	5.879	-0.377
Site 2	0.000	14.355	19.282	7.087	-0.472
Site 3	0.717	3.821	3.585	2.788	-0.066

Table 6.5: Rayleigh parameters

Site	Location	Scale
Site 1	-1.082	4.942
Site 2	-1.242	5.398
Site 3	-0.665	3.853

Table 6.6: Kappa parameters

Site	Location	Scale	Shape 1	Shape 2
Site 1	1.269	5.428	0.344	0.888
Site 2	1.519	6.160	0.413	0.819
Site 3	2.208	2.572	0.050	0.497

Figure 6.1 shows the three sites' wind speed density plots fitted with the distribution functions. The three sites have a unimodal wind speed density because it has a single peak. The Gumbel, Weibull, Wakeby, Rayleigh, and Kappa model the unimodal wind

speed density because they have a single peak. Also, the KDE and the LDE model the unimodal wind speed density because they use Gaussian kernels and basis-splines (B-splines), respectively, which can fit densities with a single peak.

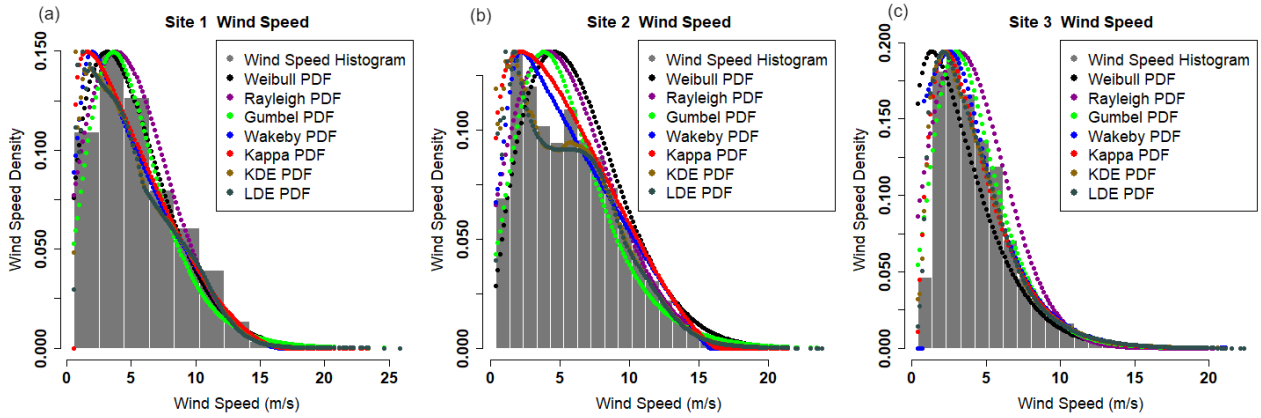

Figure 6.1: PDF modelled wind speed: (a) site 1, (b) site 2, (c) site 3

6.2.3. Wind speed spatial correlation

Table 6.7 shows the three sites Kendall's tau correlation coefficients. The wind speed's spatial correlation is assessed to determine whether the modelled wind speed maintains the measured wind speed's spatial dependency. The spatial correlation of the measured and modelled wind speed between sites 1 and 2, sites 1 and 3, and sites 2 and 3 is similar. This shows that the modelled wind speed maintains the measured wind speed's spatial dependency.

Table 6.7: Wind speed spatial correlation

Wind Speed	Sites 1 and 2 Wind Speed	Sites 1 and 3 Wind Speed	Sites 2 and 3 Wind Speed
Measured	0.295982	0.149902	0.171913
Weibull	0.295979	0.149907	0.171872
Rayleigh	0.295979	0.149907	0.171873
Gumbel	0.295979	0.149907	0.171873
Wakeby	0.295982	0.149902	0.171913
Kappa	0.295982	0.149902	0.171913
KDE	0.295982	0.149902	0.171913
LDE	0.295979	0.149907	0.171872

6.2.4. Distribution functions fit to wind speed

Figure 6.2 shows the empirical cumulative distribution functions (ECDFs) of the measured wind speed as well as the fitted Gumbel, Weibull, Wakeby, Rayleigh, Kappa, KDE, and LDE cumulative distribution functions (CDFs). The measured and modelled

wind speed ECDFs and CDFs, respectively, at the three sites have similar shapes. However, the fitted distribution functions CDFs are closer to the measured wind speeds' ECDFs at higher wind speeds than they are at lower wind speeds. This indicates that the distribution functions fit higher wind speeds better than they do lower wind speeds.

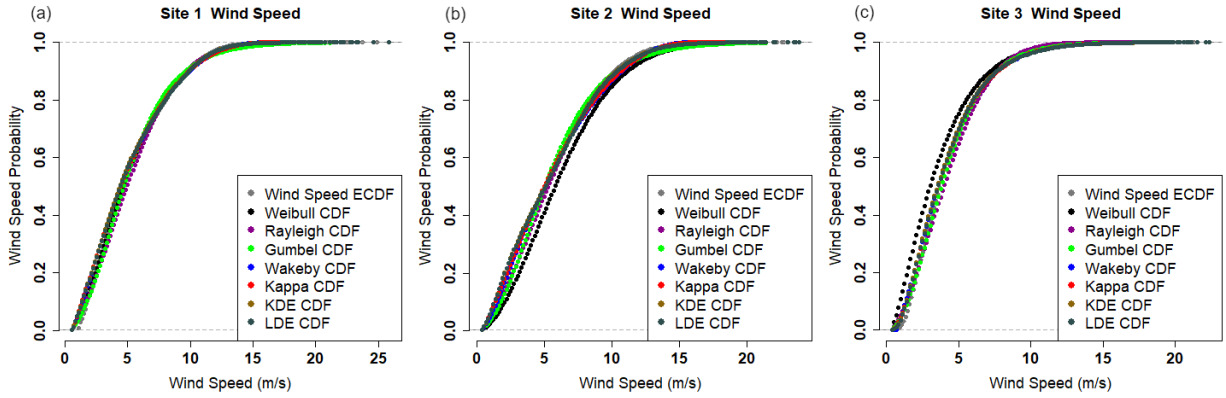

Figure 6.2: CDF modelled wind speed: (a) site 1, (b) site 2, (c) site 3

Tables 6.8 and 6.9 show the root mean square error (RMSE) and the mean absolute error (MAE) of the distribution functions fitted to the wind speed data, respectively. The results show that the KDE, followed by the LDE, has the best fit when modelling the wind speed at the three sites. The Wakeby and Kappa have the third-best and fourth-best fit, respectively, when modelling wind speed at sites 1 and 3. However, the Kappa and the Wakeby have the third-best and fourth-best fit, respectively, when modelling wind speed at site 2. The Gumbel, Weibull, and Rayleigh have the fifth-best to seventh-best fit, respectively, to wind speed at site 1. At site 2, the Gumbel, Rayleigh, and Weibull have the fifth-best to seventh-best fit, respectively, to wind speed. However, at site 3, the Rayleigh, Gumbel, and Weibull have the fifth-best to seventh-best fit, respectively, to wind speed.

Table 6.8: RMSE of distribution functions fitted to wind speed

Site	Weibull	Rayleigh	Gumbel	Wakeby	Kappa	KDE	LDE
Site 1	0.01955	0.02880	0.02744	0.00792	0.00805	0.00411	0.00744
Site 2	0.07920	0.02229	0.03160	0.01389	0.01152	0.00337	0.00652
Site 3	0.08713	0.03758	0.02713	0.01049	0.01056	0.00561	0.01000

Table 6.9: MAE of distribution functions fitted to wind speed

Site	Weibull	Rayleigh	Gumbel	Wakeby	Kappa	KDE	LDE
Site 1	0.01680	0.02427	0.02375	0.00700	0.00702	0.00325	0.00691
Site 2	0.07150	0.01600	0.02672	0.01178	0.00953	0.00237	0.00614
Site 3	0.07889	0.03310	0.02257	0.00893	0.00928	0.00489	0.00921

6.2.5. Wind speed range synthesis

Table 6.10 shows the wind speed range synthesised by the fitted Gumbel, Weibull, Wakeby, Rayleigh, Kappa, KDE, and LDE. At each site, the distribution functions synthesise different low and high wind speed values. This is because the distribution functions have different lower and upper tails that limit the low and high synthesised wind speed values. In Tables 6.1 and 6.10, comparing the low and high wind speeds from the measured and synthesised data, respectively, indicates that some of the distribution functions do not sythesise the three sites' wind speed range. At the three sites, only the Weibull and the KDE synthesise low and high wind speeds. At site 2, the Rayleigh synthesises only maximum wind speed because its upper tail extends to the site's maximum wind speed. However, the Rayleigh synthesises negative low wind speed at the three sites. The Gumbel synthesises maximum wind speed at the three sites, however, it also synthesises negative low wind speed. The synthesis of negative wind speed by the Rayleigh and the Gumbel indicates that they do not model low wind speed at the three sites because the low wind speed should be positive, as shown in Table 6.1. The Wakeby synthesises low wind speed at sites 1 and 2, while at site 3 it synthesises maximum wind speed only. The Kappa synthesises the wind speed range at site 3, while it does not synthesise both low and high wind speed at site 1, and at site 2 it synthesises low wind speed only. The LDE synthesises the wind speed range at sites 2 and 3, and at site 1 it synthesises low wind speed only. The ability of the distribution functions to synthesise the wind speed range is due to their lower and upper tails extending to low and high wind speed values at the three sites.

Table 6.10: Synthesised wind speed ranges

Sites	Statistic	Weibull	Rayleigh	Gumbel	Wakeby	Kappa	KDE	LDE
Site 1	High (m/s)	28.039	23.698	36.500	16.325	16.818	25.981	25.454
	Low (m/s)	0.002	-1.068	-2.990	0.501	0.612	0.411	0.047
Site 2	High (m/s)	28.709	26.319	41.138	15.735	16.369	24.058	24.677
	Low (m/s)	0.009	-1.226	-3.306	0.000	0.238	0.292	0.004
Site 3	High (m/s)	26.042	19.005	29.576	26.087	26.904	22.572	25.679
	Low (m/s)	0.000	-0.663	-2.782	0.717	0.377	0.243	0.000

6.3. Wind power generation impact on transient stability

6.3.1 Power produced by wind power generators

Three WPGs are integrated into the IEEE 9-bus test system at buses 5, 6, and 8, as shown in Figure 4.1. The variable power produced by the WPGs at buses 5, 6, and 8 is developed using the sites 1, 2, and 3 wind speed, respectively. The wind speed is converted to the power produced by the WPGs using the Enercon E-82 E2, 2.05 MW wind turbine power curve shown in Figure 6.3. The Weibull CDF is used to model the shape of the Enercon wind turbine power curve. The fitted Weibull CDF has a shape and scale parameter of 4.081 and 9.097, respectively. The variable power produced by each of the three WPGs is modelled by converting the measured and modelled variable wind speed at the WPGs' locations to power using the fitted Weibull CDF.

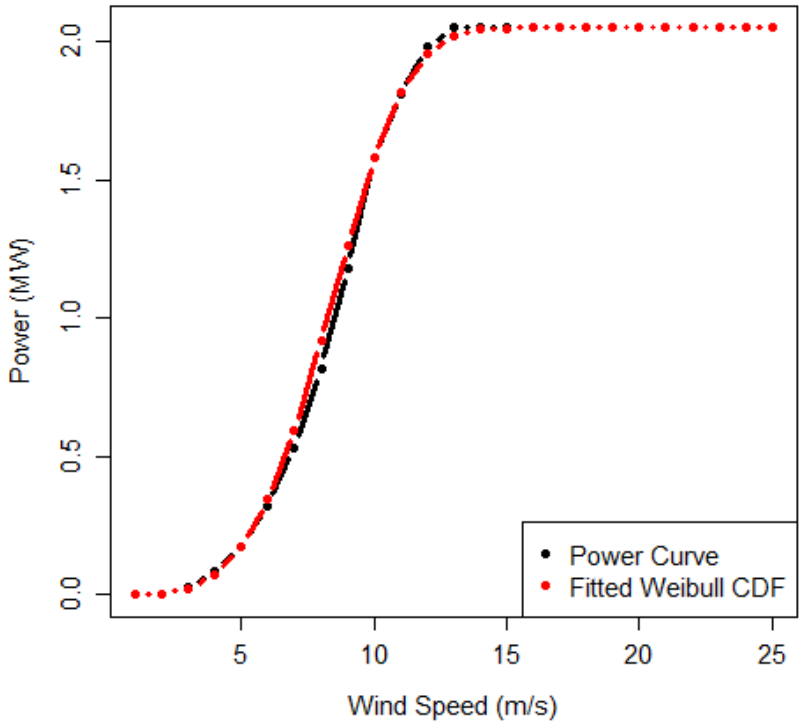

Figure 6.3: Wind turbine power curve modelling

6.3.2. Wind power generation production sample size

Monte-Carlo Simulations is used to randomly sample 5000 samples from each of the WPGs' active power values developed using measured and modelled wind speed. Figures 6.4 to 6.6 show the sampled WPGs 1, 2 and 3 normalised turbine power

production moving means, respectively. The law of large numbers given by equation (3.17) is used to determine the required sample size, which is quantified based on the number of samples required for the normalised turbine power production moving mean to stabilise. About 2787 samples are required for the normalised turbine power production moving means of WPGs 1 and 2 to stabilise, while about 4180 samples are required for WPG 3's normalised turbine power production moving mean to stabilise. A minimum of about 4180 samples is required to ensure that each of the WPGs' normalised turbine power production moving means stabilise. In this study, the probabilistic method is used to assess power system transient stability using 5000 samples of the power produced by the three WPGs.

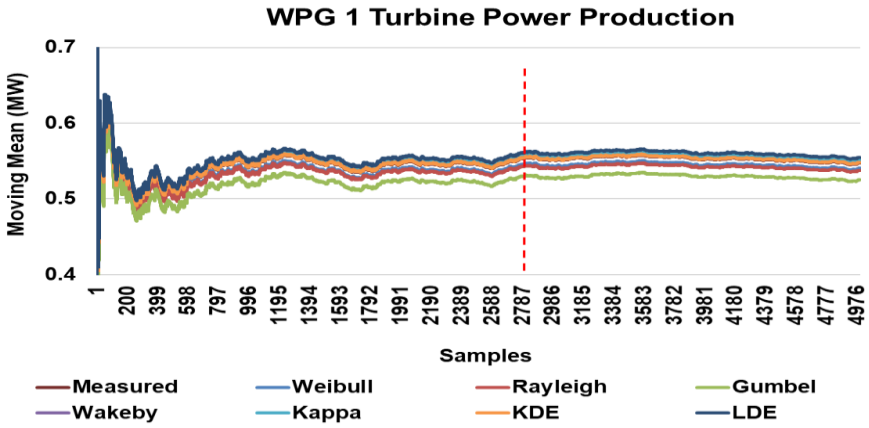

Figure 6.4: WPG 1 normalised power production moving mean

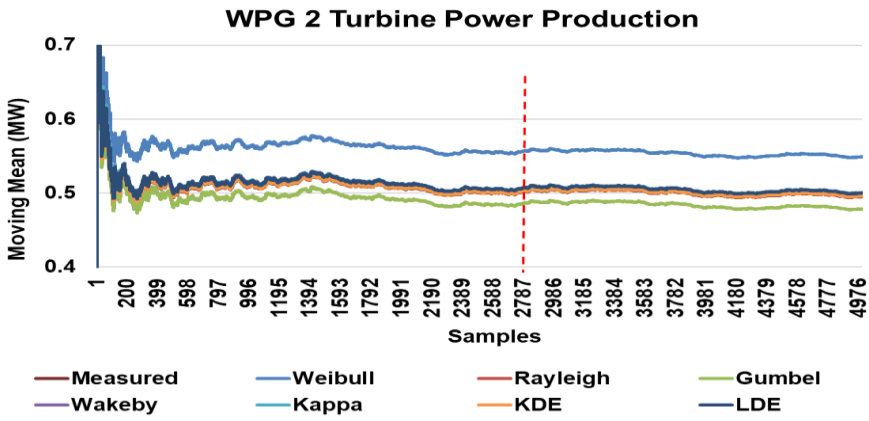

Figure 6.5: WPG 2 normalised power production moving mean

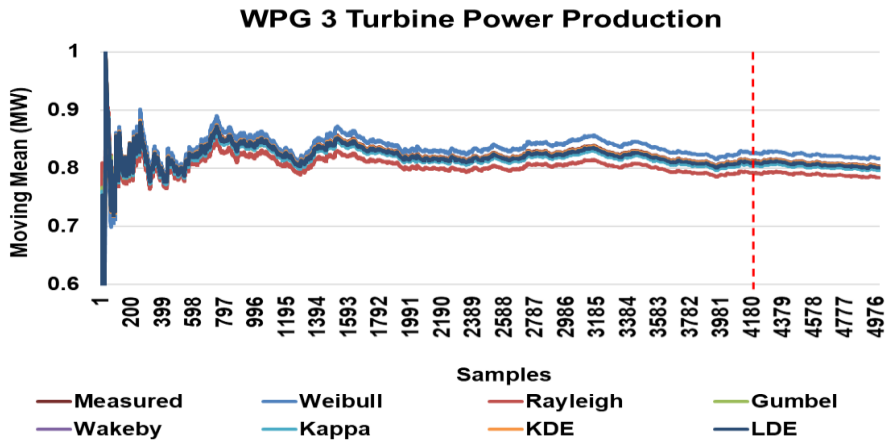

Figure 6.6: WPG 3 normalised power production moving mean

6.3.3. Wind power generation impact on transient stability

For each of the 5000 power production samples for WPGs 1, 2, and 3, probabilistic studies are performed to investigate their impact on the IEEE 9-bus test system's transient stability. The test system's transient stability is investigated by applying three-phase faults sequentially on line 6-9 and line 8-9, close to bus 9. During the analysis, Gen 3's rotor angle deviations are monitored. Figure 6.7 shows Gen 3's maximum rotor angle deviation ECDFs. The results show that developing the power produced by the WPGs using the measured and modelled wind speed produces Gen 3's maximum rotor angle ECDFs with similar shapes.

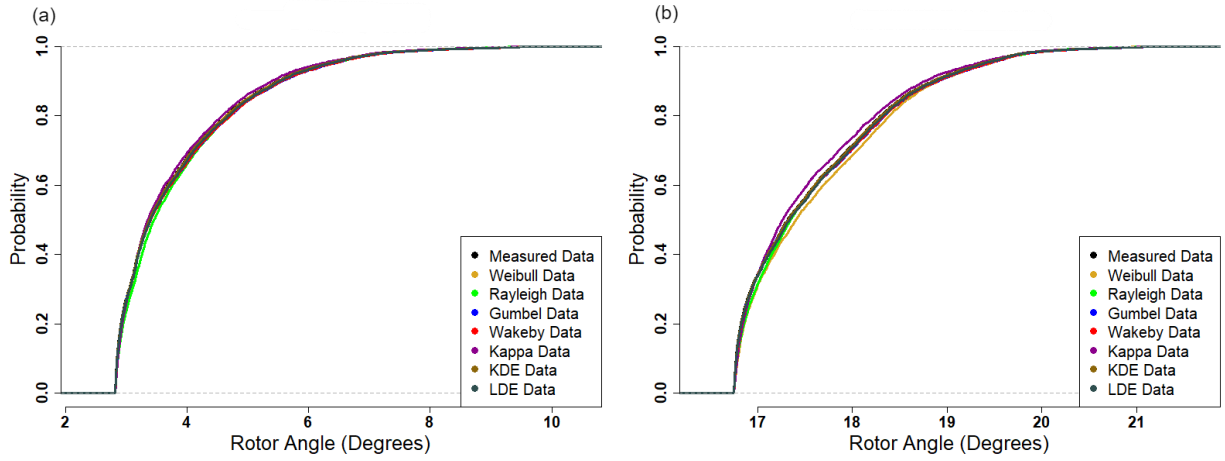

Figure 6.7: Gen 3 maximum rotor angle deviation ECDFs owing to wind power generation variability when faults were applied close to bus 9 on: (a) line 6-9, (b) line 8-9

Tables 6.11 and 6.12 show the respective RMSE and MAE results that compare Gen 3's maximum rotor angle deviation ECDFs obtained using measured and modelled wind speed. The results show that wind speed modelled by the KDE, LDE and Kappa results in Gen 3's maximum rotor angle deviation ECDFs with the best, second-best, and third-best RMSE and MAE, respectively.

Table 6.11: Gen 3 maximum rotor angle deviation ECDFs RMSE owing to modelled power

Fault	Weibull Data	Rayleigh Data	Gumbel Data	Wakeby Data	Kappa Data	KDE Data	LDE Data
Line 6-9	0.036437	0.015180	0.016763	0.008582	0.007776	0.001212	0.002598
Line 8-9	0.031970	0.011322	0.015659	0.006288	0.005881	0.000858	0.001852

Table 6.12: Gen 3 maximum rotor angle deviation ECDFs MAE owing to modelled power

Fault	Weibull Data	Rayleigh Data	Gumbel Data	Wakeby Data	Kappa Data	KDE Data	LDE Data
Line 6-9	0.027182	0.011476	0.011148	0.005842	0.005528	0.000868	0.001858
Line 8-9	0.024045	0.008307	0.010222	0.004991	0.004608	0.000617	0.001283

Figures 6.8 to 6.10 show the reactive power injected by the WPGs during system faults when the power they produce is developed using measured wind speed and wind speed modelled by the KDE and LDE, respectively. The diagrams of the reactive power injected by the WPGs when the power they produce is modelled using the Gumbel, Weibull, Wakeby, Rayleigh, and Kappa are shown in Appendix B. It can be seen that during the faults, the WPGs inject reactive power to support the test system's voltages. Once the applied faults are isolated, the WPGs reduce the reactive power they inject into the test system.

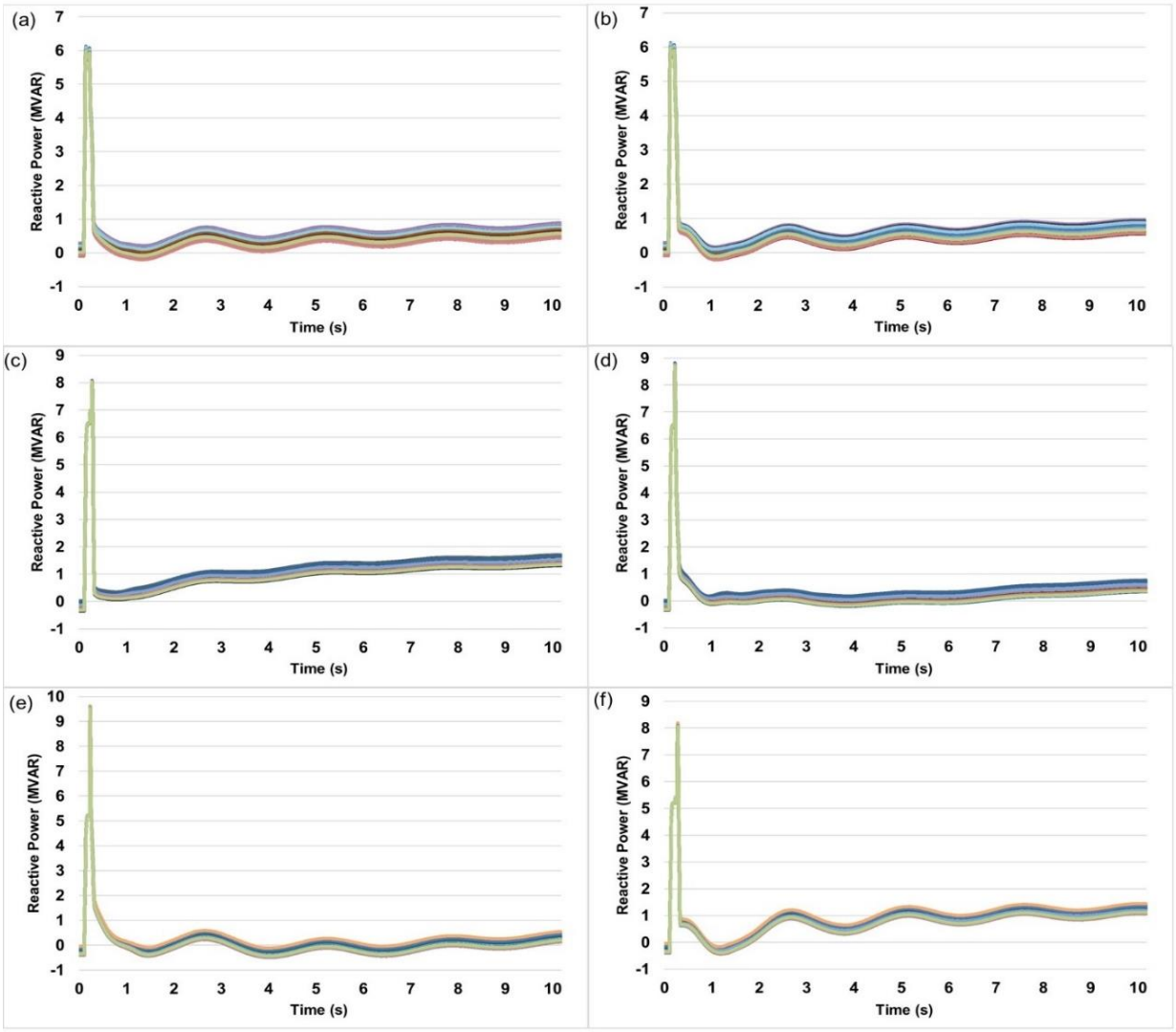

Figure 6.8: WPGs' reactive power injection with power production developed using measured wind speed: (a) WPG1 reactive power with the fault applied on line 6-9, (b) WPG1 reactive power with the fault applied on line 8-9, (c) WPG2 reactive power with the fault applied on line 6-9, (d) WPG2 reactive power with the fault applied on line 8-9, (e) WPG3 reactive power with the fault applied on line 6-9, and (f) WPG3 reactive power with the fault applied on line 8-9

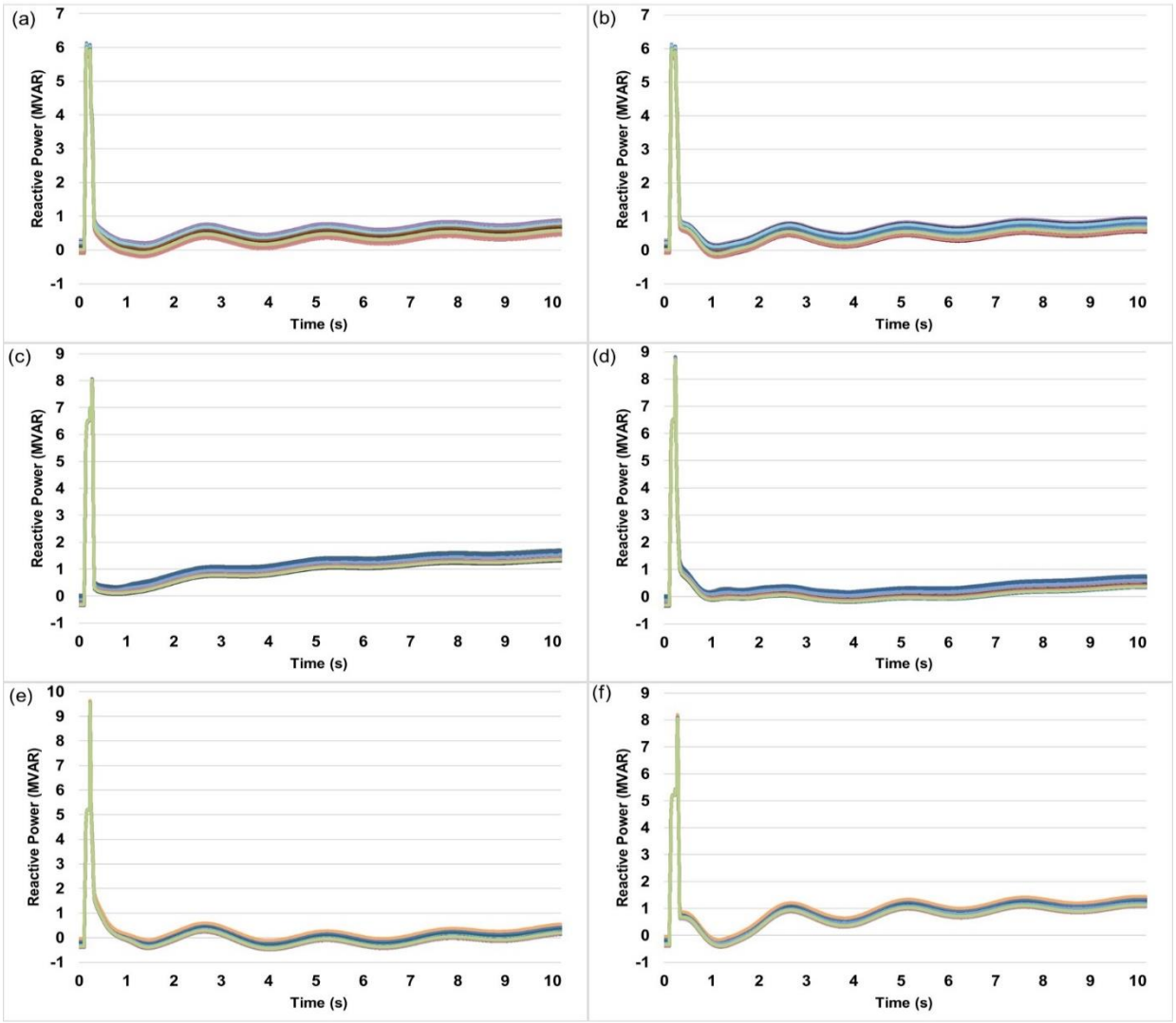

Figure 6.9: WPGs' reactive power injection with power production developed using wind speed modelled by the KDE distribution function: (a) WPG1 reactive power with the fault applied on line 6-9, (b) WPG1 reactive power with the fault applied on line 8-9, (c) WPG2 reactive power with the fault applied on line 6-9, (d) WPG2 reactive power with the fault applied on line 8-9, (e) WPG3 reactive power with the fault applied on line 6-9, and (f) WPG3 reactive power with the fault applied on line 8-9

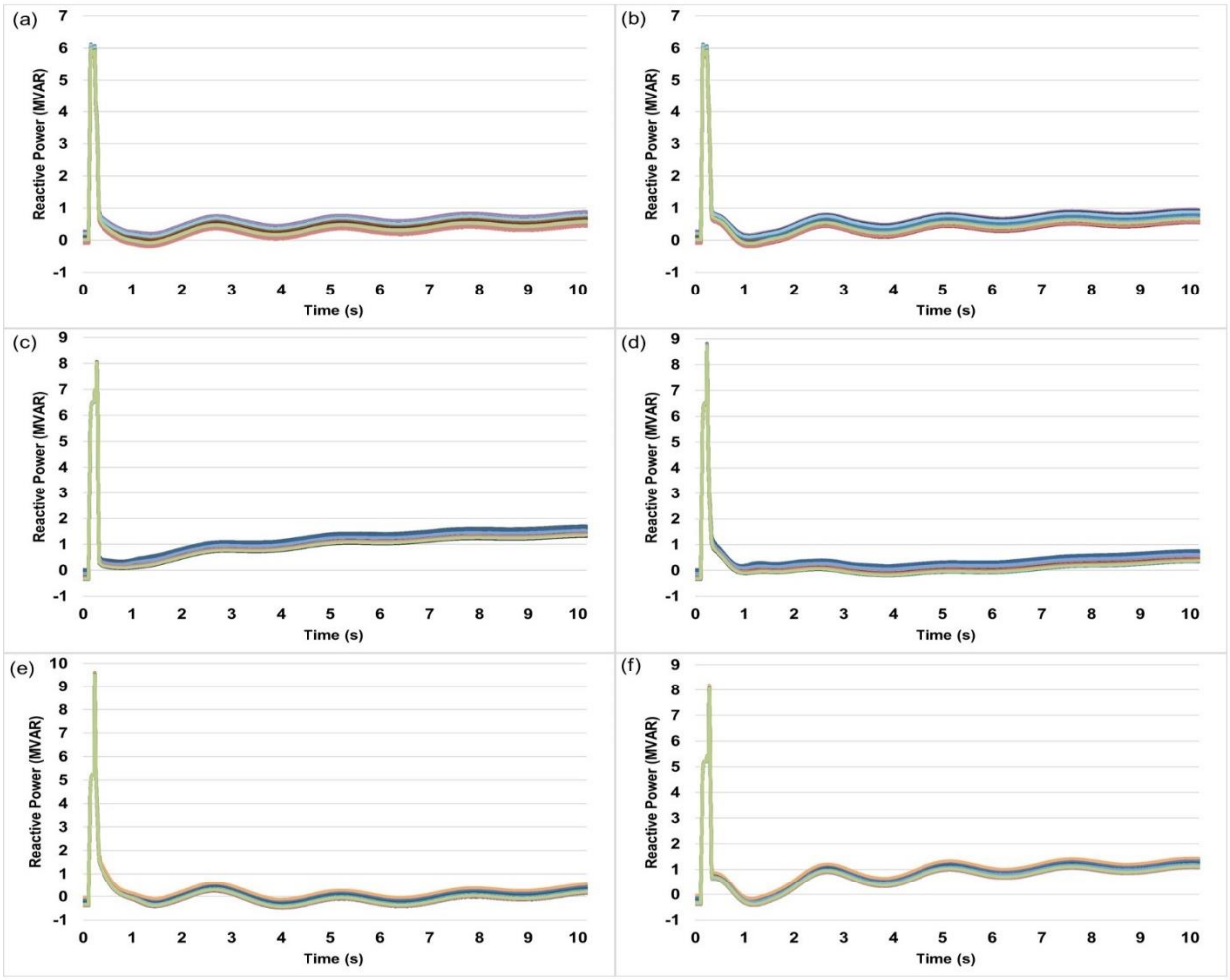

Figure 6.10: WPGs' reactive power injection with power production developed using wind speed modelled by the LDE distribution function: (a) WPG1 reactive power with the fault applied on line 6-9, (b) WPG1 reactive power with the fault applied on line 8-9, (c) WPG2 reactive power with the fault applied on line 6-9, (d) WPG2 reactive power with the fault applied on line 8-9, (e) WPG3 reactive power with the fault applied on line 6-9, and (f) WPG3 reactive power with the fault applied on line 8-9

6.4. Discussion of results

In section 6.2, wind speed from three South Africa measurements sites is modelled using the Gumbel, Weibull, Wakeby, Rayleigh, Kappa, LDE and KDE. The results in Table 6.7 show that modelling the wind speed using the distribution functions preserves the spatial correlation of the measured wind speed at the three sites. The results in Tables 6.8 and 6.9 show that distribution functions such as the KDE and the LDE, whose shapes are not defined by parameters, fit wind speed density better than distribution functions such as the Gumbel, Weibull, Wakeby, Rayleigh, and Kappa, whose shapes are defined by parameters. Unlike distributions functions that have parameters, those without parameters do not have a limitation on the wind speed density shapes they can model.

A comparison of Tables 6.1 and 6.10 shows that only the KDE and Weibull model the wind speed range at the three sites. The Gumbel, Wakeby, Rayleigh, Kappa, and LDE do not synthesise low and high wind speed values at all the sites. These findings highlight the importance of assessing the distribution functions' wind speed range modelling ability. As a result, selecting distribution functions based on their fit only does not ensure that they also synthesise the wind speed range.

In section 6.3, the impact of the variable power produced by WPGs on the IEEE 9-bus test system's transient stability is assessed. The variable power produced by the WPGs is developed using the measured and modelled wind speed. The results in Tables 6.11 and 6.12 show that wind speed modelled by distribution functions such as the KDE and the LDE cause the power system to have similar transient stability to that observed when measured wind speed is used. However, distribution functions such as the Gumbel, Weibull, Wakeby, Rayleigh, and Kappa result in the power system transient stability being dissimilar to that observed when measured wind speed is used. This is because the KDE and the LDE fit the wind speed density better than the Gumbel, Weibull, Wakeby, Rayleigh, and Kappa. This shows that the KDE and the LDE are good candidates for modelling wind speed density.

6.5. Summary

In this chapter, wind speed variability from three sites was modelled using seven distribution functions consisting of the Gumbel, Weibull, Wakeby, Rayleigh, Kappa, KDE, and LDE. The distribution functions were assessed on the basis of their fit and wind speed range modelling ability at each site. The wind speed was converted to the power produced by three WPGs located in the IEEE 9-bus test system. The Enercon E-82 E2, 2.05 MW wind turbine power curve was used to convert the wind speed to power produced by the WPGs. It was found that the KDE and the LDE have the best fit to wind speed. It was also found that some of the distribution functions such as the Gumbel, Wakeby, Rayleigh, Kappa, and LDE, did not synthesise low and high wind speed values at all the sites. Investigating the impact of the variable power produced by the WPGs on the transient stability of the IEEE 9-bus test system showed that wind speed modelled using the KDE and the LDE caused the system to have similar transient stability as those produced when measured wind speed was used.

CHAPTER 7: TRANSIENT STABILITY ASSESSMENT USING THE DETERMINISTIC AND PROBABILISTIC METHODS

7.1. Introduction

In the previous chapter, wind speed variability from three South African wind speed measurement sites was modelled using seven distribution functions. The wind speed was then used to develop the variable power produced by three wind power generators (WPGs) integrated into the IEEE 9-bus test system. Furthermore, the impact of the power produced by the WPGs on the test system's transient stability was then assessed. In this chapter, power system transient stability is assessed using the deterministic and probabilistic methods. The two methods are used to investigate the impact of increasing the load and varying the power produced by WPGs on the transient stability of the IEEE 9-bus test system.

7.2. Deterministic power system transient stability

7.2.1 Deterministic method power system scenarios

The deterministic analysis of transient stability entails developing a few power system operating conditions which are then used to assess stability. The deterministic assessment of the IEEE 9-bus test system's transient stability is performed using the scenarios shown in Table 7.1. Overall, nine scenarios are developed for the study. Scenarios 1 to 3, 4 to 6, and 7 to 9 represent the low, moderate, and peak system loading conditions, respectively. During the low, moderate, and peak system loading conditions, the total system load is set to 20%, 60%, and 100%, respectively, of peak system demand. During each of the three system loading conditions developed, the power produced by the three WPGs is also set to 20%, 60%, and 100%, of their peak generation capacity. This is done to develop power system operating conditions with different wind power generation penetration levels and system net-loading conditions. The developed power system operating conditions are used to assess the impact of wind power generation penetration levels and system net-loading on power system transient stability.

Table 7.1: Study scenarios

Scenario	Bus 5 (MW)	Bus 6 (MW)	Bus 8 (MW)	WPG 1 (MW)	WPG 2 (MW)	WPG3 (MW)
1	25	18	20	2.05	2.05	2.05
2	25	18	20	6.15	6.15	6.15
3	25	18	20	10.25	10.25	10.25
4	75	54	60	2.05	2.05	2.05
5	75	54	60	6.15	6.15	6.15
6	75	54	60	10.25	10.25	10.25
7	125	90	100	2.05	2.05	2.05
8	125	90	100	6.15	6.15	6.15
9	125	90	100	10.25	10.25	10.25

Figure 7.1 shows the resulting wind power generation penetration levels and system net-load for each of the nine scenarios developed. The wind power generation penetration level and the system net-load for each scenario are quantified using equations (3.18) and (3.19), respectively. The wind power generation penetration level is maximum when the total system load is low, while the power produced by the WPGs is high. The inverse is true for the low wind power generation penetration level. Scenario 3 has the highest wind power generation penetration level (48.81%) because the total system load is at 20% of peak demand, while the power produced by the WPGs is at 100% of their generation capacity. On the other hand, scenario 7 has the lowest wind power generation penetration level (1.95%) because the total system load is at 100% of its peak demand, while the power produced by the WPGs is at 20% of their generation capacity. Scenarios 1, 5, and 9 each have a wind power generation penetration level of 9.76%. This indicates that different power system operating conditions with different loading conditions and wind power generation power production conditions can produce similar wind power generation penetration levels. This is because the penetration level, as seen in equation (3.18), is based on the ratio between the total system load and the total power produced by WPGs in a power system.

It can also be seen in Figure 7.1 that Scenario 3, which has the highest wind power generation penetration level (48.81%), results in a system net-load of 32 MW. On the other hand, scenario 7, which has the lowest wind power generation penetration level (1.95%) has a system net-load of 309 MW. This shows that the system net-load reduces when the wind power generation penetration level increases. This is because a larger

proportion of the system load is supplied by the WPGs when the power they produce increases.

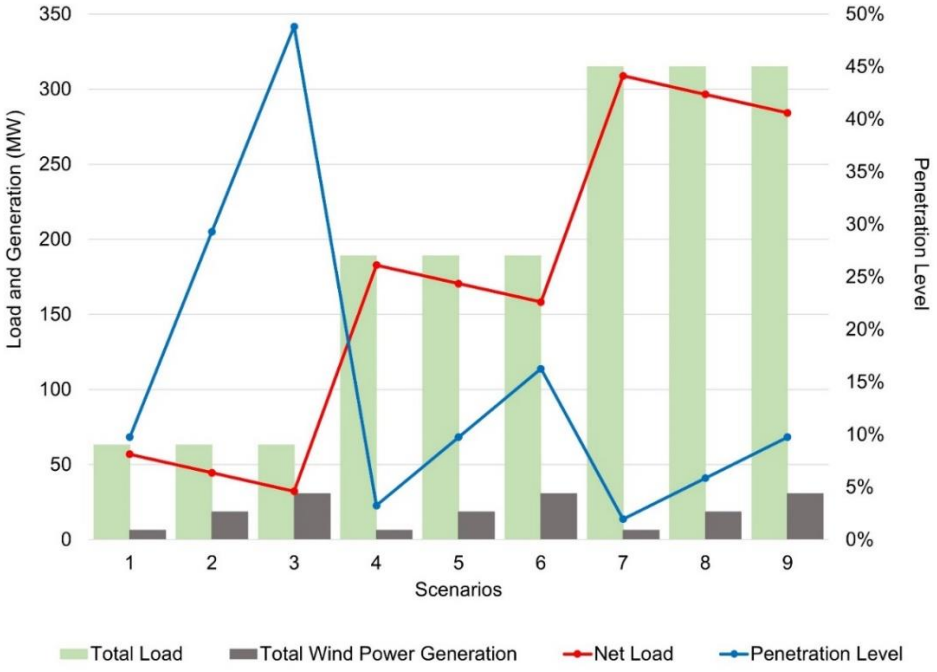

Figure 7.1: Wind power generation penetration level and system net-load

7.2.2 Deterministic power system transient stability results

The IEEE 9-bus test system's transient stability is assessed by applying three-phase faults sequentially on line 6-9 and on line 8-9, close to bus 9. Table 7.2 shows the study's results. During low (scenarios 1 to 3), moderate (scenarios 4 to 6) and maximum (scenarios 7 to 9) system loading conditions, increasing the power produced by the WPGs increases the wind power generation penetration level and reduces the system net-load. In scenarios 1 to 3, the wind power generation penetration level increases from 9.76% to 48.81%, while the system net-load reduces from 57 MW to 32 MW. In scenarios 4 to 6, the wind power generation penetration level increases from 3.25% to 16.27%, while the system net-load reduces from 183 MW to 158 MW. Also, in scenarios 7 to 9, the wind power generation penetration level increases from 1.95% to 9.76%, while the system net-load reduces from 309 MW to 284 MW. The reduction in the system net-load results in Gen 3's maximum rotor angle deviations increasing, thereby reducing the system's transient stability.

Table 7.2: WPGs penetration levels, system net-load, and Gen 3 maximum rotor angle deviations

Scenario	Total Load (MW)	Total Wind Power Generation (MW)	Penetration Level	Net-Load (MW)	Fault on line 6-9	Fault on line 8-9
1	63	6.15	9.76%	57	88.18^0	84.11^0
2	63	18.45	29.29%	45	91.92^0	87.35^0
3	63	30.75	48.81%	32	95.80^0	90.62^0
4	189	6.15	3.25%	183	43.28^0	45.69^0
5	189	18.45	9.76%	171	47.03^0	48.72^0
6	189	30.75	16.27%	158	50.99^0	51.93^0
7	315	6.15	1.95%	309	3.96^0	17.62^0
8	315	18.45	5.86%	297	6.54^0	19.39^0
9	315	30.75	9.76%	284	9.95^0	21.32^0

Referring to Table 7.2, it can also be seen that reducing the system load, while maintaining the power produced by the WPGs constant (scenarios 7, 4, and 1, scenarios 8, 5, and 2, and scenarios 9, 6, and 3), results in Gen 3's maximum rotor angle deviations increasing. In scenarios 7, 4, and 1, the wind power generation penetration level increases from 1.95% to 9.76%, and the system net-load reduces from 309 MW to 57 MW. In scenarios 8, 5, and 2, the wind power generation penetration level increases from 5.86% to 29.29%, and the system net-load reduces from 297 MW to 45 MW. Also, in scenarios 9, 6, and 3, the wind power generation penetration level increases from 9.76% to 48.81%, and the system net-load reduces from 284 MW to 32 MW. These results show that increasing the wind power generation penetration level reduces the system's net-load, resulting in reduced transient stability.

In Table 7.2, scenarios 1, 5, and 9 have a wind power generation penetration level of 9.76%. However, the same scenarios have system net-loads of 57 MW, 171 MW, and 284 MW, respectively. Also, among the three scenarios, scenario 9 has the lowest Gen 3 maximum rotor angle deviations, followed by scenario 5 and then scenario 1. These results show that power system operating conditions with similar wind power generation penetration levels can result in different transient stability. The results also show that the reduction in the power system's net-load results in reduced power system transient stability.

7.3. Probabilistic power system transient stability

7.3.1 Probabilistic method power system scenarios

The probabilistic assessment of power system transient stability is conducted using numerous samples of power produced by the three WPGs integrated into the IEEE 9-bus test system. The system load, like in section 7.2 where the deterministic method is used, is maintained at 20%, 60%, and 100% of peak demand to model low, moderate, and peak loading conditions, respectively. The 5000 samples of power developed for the three WPGs from measured wind speed in Chapter 6 are used in this investigation. The numerous power system operating conditions are developed to create system operating conditions with various wind power generation penetration levels and system net-loading. They are used to assess the impact of varying levels of wind power generation penetration and varying system net-loading on transient stability. For each of the three loading conditions and the 5000 samples of power produced by the WPGs, probabilistic studies are performed to assess the IEEE 9-bus test system's transient stability. Three-phase faults are applied sequentially on line 6-9 and line 8-9, close to bus 9, and Gen 3's maximum rotor angle deviations are monitored.

7.3.2 Probabilistic power system transient stability results

Figures 7.2 and 7.3 show scatter plots of the wind power generation penetration level against Gen 3's maximum rotor angle deviations when faults are applied on line 6-9 and line 8-9, respectively, during low, moderate, and peak system loading conditions. The wind power generation penetration level is quantified using equation (3.18). When faults are applied on line 6-9, Gen 3's maximum rotor angle deviations range between 86.52^0 and 95.77^0 during low system loading conditions. During moderate system loading conditions, Gen 3's maximum rotor angle deviations range between 41.61^0 and 50.95^0, and they range between 2.82^0 and 9.91^0 during peak system loading conditions. When faults are applied on line 8-9, Gen 3's maximum rotor angle deviations range between 82.61^0 and 90.60^0 during low system loading conditions. During moderate system loading conditions, Gen 3's maximum rotor angle deviations range between 44.27^0 and 51.90^0, and they range between 16.75^0 and 21.30^0 during peak system loading

conditions. These results show that increasing the system load reduces Gen 3's maximum rotor angular deviations, thereby improving the power system's transient stability. Also, in Figures 7.2 and 7.3 there is a directly proportional relationship between the wind power penetration level and Gen 3's maximum rotor angle deviations. These results show that increasing the penetration level of WPGs in a power system reduces the system's transient stability.

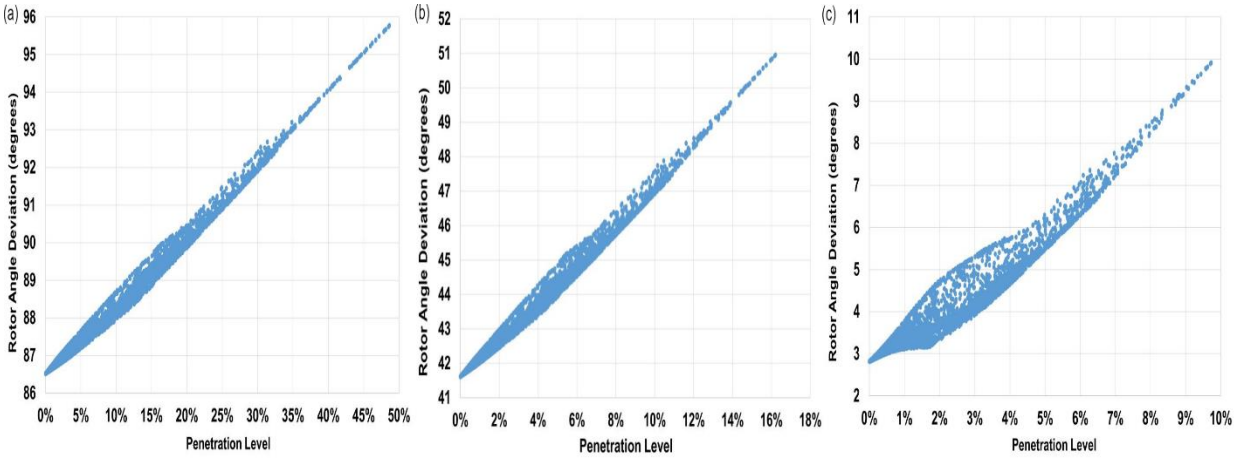

Figure 7.2: Scatter plots of the penetration level of WPGs against Gen 3 maximum rotor angle deviations when faults were applied on line 6-9: (a) low system loading, (b) moderate system loading, (c) peak system loading

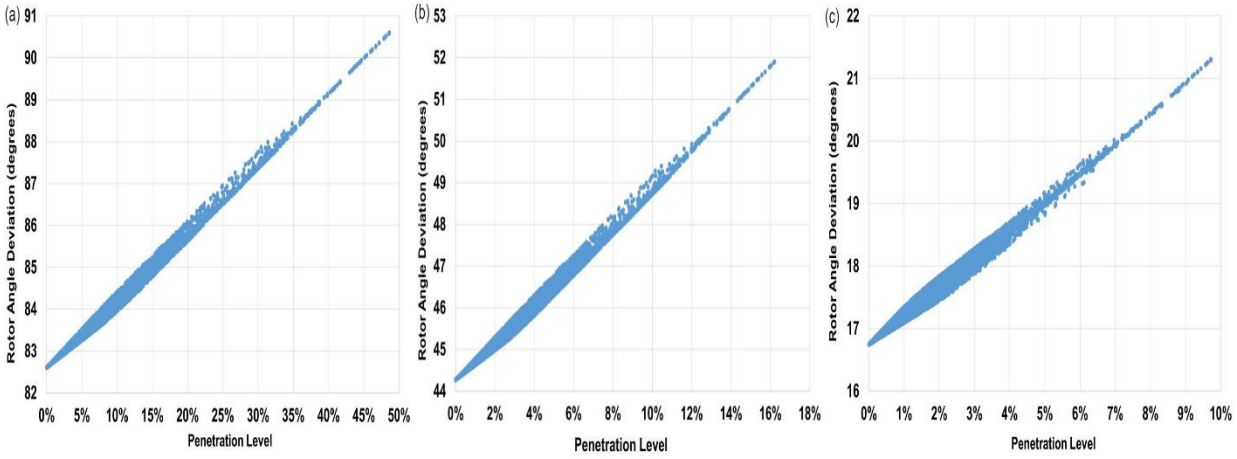

Figure 7.3: Scatter plots of the penetration level of WPGs against Gen 3 maximum rotor angle deviations when faults were applied on line 8-9: (a) low system loading, (b) moderate system loading, (c) peak system loading

Figures 7.4 and 7.5 show scatter plots of the system's net-load against Gen 3's maximum rotor angle deviations when faults are applied on line 6-9 and line 8-9, respectively, during low, moderate, and peak system loading conditions. Equation (3.19) is used to quantify the system net-load. When the system load increases from low to peak loading conditions, the system's net-load also increases. It can also be seen that there is an inversely proportional relationship between the system net-load and Gen 3's maximum rotor angle deviations. These results show that the power system's transient stability reduces because of the reduction in the system's net-load caused by the increased power produced by the WPGs.

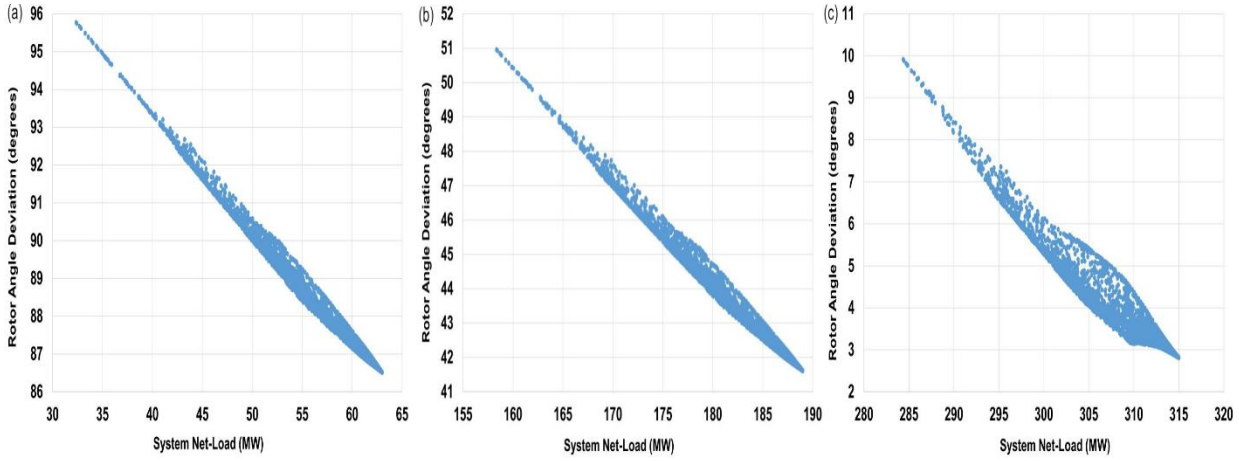

Figure 7.4: Scatter plot of the system net-load against Gen 3's maximum rotor angle deviations when faults were applied on line 6-9 during: (a) low system loading, (b) moderate system loading, (c) peak system loading

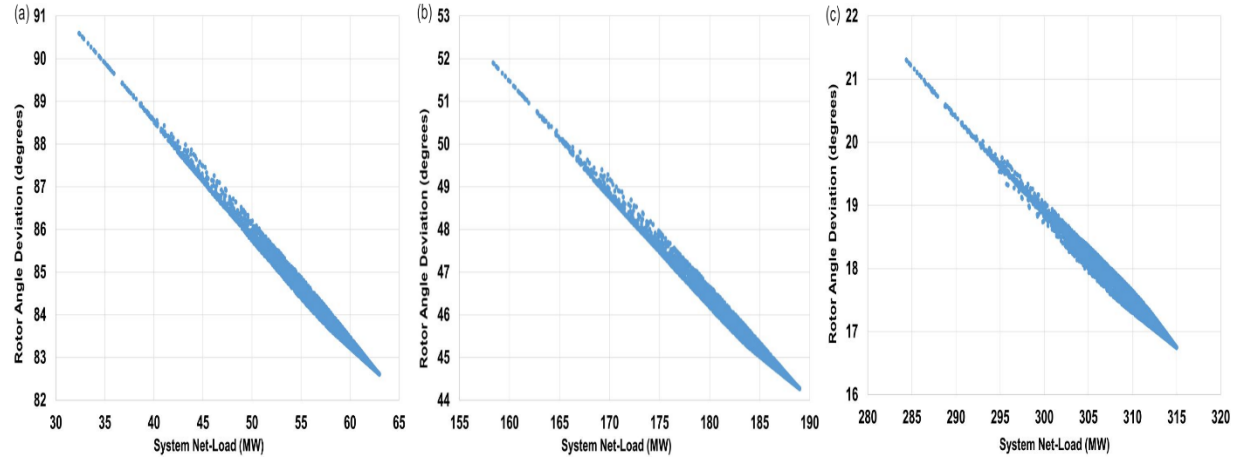

Figure 7.5: Scatter plot of the system net-load against Gen 3's maximum rotor angle deviations when faults were applied on line 8-9 during: (a) low system loading, (b) moderate system loading, (c) peak system loading

7.4. Discussion of results

In section 7.2, the transient stability of the IEEE 9-bus test system is assessed using the deterministic method. The power system's stability is assessed using nine scenarios of load and power produced by the WPGs. In section 7.3, the probabilistic method is used to assess the transient stability of the IEEE 9-bus test system. The power system's transient stability is assessed using three system loading conditions and 5000 scenarios of power produced by the WPGs.

Table 7.2, and Figures 7.2 and 7.3 show that when using the deterministic and probabilistic methods, respectively, when the load is increased, Gen 3's maximum rotor angle deviations reduce when faults are applied. This indicates that increasing the system load improves power system transient stability. These results show that when assessing the transient stability of a power system with integrated WPGs, the system's low loading conditions should be used as they result in the worst system operating conditions for transient stability. It can also be seen in Table 7.2, and Figures 7.2 and 7.3 that increasing the wind power generation penetration level increases Gen 3's maximum rotor angle deviations. These results indicate that the power system's transient stability reduces when the wind power generation penetration level increases.

Table 7.2, and Figures 7.4 and 7.5 show that when using the deterministic and probabilistic methods, respectively, reducing the system's net-load results in increasing Gen 3's maximum rotor angle deviations, thus reducing the power system's transient stability. The system's net-load reduces when the power produced by the WPGs increases. Increasing the power produced by the WPGs results in a larger proportion of the system load being supplied by the WPGs, causing the system's net-load to reduce. These results show that when assessing the transient stability of a power system integrating WPGs, scenarios in which the system net-load is low should be used since they result in the worst system operating conditions for transient stability.

7.5. Summary

In this chapter, the impact of the variable power produced by WPGs on the transient stability of the IEEE 9-bus test system was assessed using the deterministic and probabilistic methods. When using the deterministic and probabilistic methods, three system loading conditions were assessed, namely, low, moderate, and peak loading. Also, when using the deterministic method, three wind power generation scenarios were investigated, and 5000 wind power generation scenarios were investigated when using the probabilistic method. When using both methods, it was found that increasing the system load improved power system transient stability. It was also found that increasing the penetration level of WPGs reduced the system's net-load, causing the power system to operate closer to transient instability.

CHAPTER 8: CONCLUSION

8.1. Research conclusion

In this research, load and wind speed variability modelling using distribution functions has been presented. The distribution functions were selected based on their fit and their ability to model the data range. Also, the transient stability of a power system integrating fully-rated converter wind power generators (WPGs) was investigated using deterministic and probabilistic methods. The load and wind speed variability were modelled using seven distribution functions each. The load was modelled using the parametric Gaussian, Rayleigh, Wakeby, Kappa and Gaussian Mixture Model (GMM), and the non-parametric Kernel density estimation (KDE) and Logspline density estimation (LDE). While the wind speed was modelled using the parametric Rayleigh, Weibull, Wakeby, Gumbel and Kappa, and the non-parametric KDE and LDE. It was found that only the KDE and LDE had a good fit and modelled the load range for all the loads. It was also found that only the Weibull and KDE modelled the wind speed range at all the sites. However, only the KDE and LDE had a good fit to the wind speed at all the sites. These findings show that not all distribution functions can synthesise the range of the data they are modelling. Based on these findings, distribution functions should be selected based on their fit and their ability to model the data range to ensure that they can synthesise both low and high values. In this research, the distribution functions' ability to synthesise the data range ensures that the load they synthesise can model low and high power system loading conditions. It also ensures that the wind speed they synthesise when converted to the power produced by WPGs can model low and high power production conditions.

In addition to selecting distribution functions for modelling purposes, the impact of the modelled load and wind speed on the IEEE 9-bus test system's transient stability was assessed. The power produced by WPGs integrated into the test system was developed using the wind speed. It was found that the load modelled using the KDE and the LDE produced transient stability results that were similar to those produced when measured load was used. It was also found that wind speed modelled using the KDE and LDE resulted in the WPGs producing power that caused the test system to have similar

transient stability results to those produced when measured wind speed was used. These results show that the KDE and the LDE can be used to model load and wind speed variability in power systems integrating WPGs. This finding highlight that when modelling load and wind speed variability, in addition to the commonly used distribution functions, the KDE and LDE should also be considered because the data they synthesise can result in similar power system transient stability results as those produced when measured load and wind speed are used.

Furthermore, the deterministic and probabilistic methods were used to investigate the impact of the variable power produced by fully-rated converter WPGs on the transient stability of the IEEE 9-bus test system. Using both methods, it was found that when the system load increased, the power system's transient stability improved. An increase in power system load improves transient stability because synchronous generation operates with a larger margin to instability than when system load reduces. It was also found that when the power produced by WPGs increased, the power system's net-load reduced, and this resulted in the power system's transient stability also reducing. A low system net-load reduces transient stability because synchronous generation operates with a reduced margin to instability than when the system net-load is larger. These findings highlight the fact that the transient stability of power systems integrating WPGs should be studied using scenarios in which the power produced by WPGs is high, during periods when the system load is low. These scenarios can result in low system net-loading, causing synchronous generators to operate closer to transient instability, thereby increasing the risk the power system becomes transiently unstable should faults occur in the system.

8.2. Future research

It is recommended that future research investigate why a power system operates closer to transient instability when its net-load reduces because of the increased power produced by WPGs. Also, it is recommended that future research investigates system loading and wind power generation conditions that increase the risk of power system small-signal, voltage, and frequency instability.

REFERENCES

[1] United Nations, "The sustainable development goals report: 2020," United Nations, 2020. Accessed: 14 August 2020. [Online]. Available: https://unstats.un.org/sdgs/report/2020/The-Sustainable-Development-Goals-Report-2020.pdf

[2] J. Lee,and F. Zhao, "Global wind report 2022," Global Wind Energy Council, 2022. Accessed: 16 April 2022. [Online]. Available: https://gwec.net/global-wind-report-2022/

[3] A. A. Arfoa, "High renewable energy penetration impact on voltage and transient stability," *Jordan Journal of Electrical Engineering,* vol. 3, no. 1, pp. 75-85, 2017.

[4] B. Wang, L. Zhu, and D. Chen, "Mechanism research on the influence of large scale wind power integration on power system angle stability," *Energy Procedia,* vol. 145, no. 1, pp. 295-300, 2018.

[5] C. Lackner, F. Wilches-Bernal, and J. H. Chow, "Effects of wind generation integration on power system transient stability," in Proceedings of the IEEE Power & Energy Society General Meeting (PESGM), Portland, United States of America, 5-10 August, 2018.

[6] S. A. Kusumo, Tiyono, and L. M. Putranto, "Transient stability study in grid integrated wind farm," in Proceedings of the 5th International Conference on Information Technology, Computer, and Electrical Engineering, Semarang, Indonesia, 27-28 September, 2018.

[7] S. Vijayshankar, V. Purba, P. J. Seiler, and S. V. Dhople, "Impact of increasing the number of type-3 wind turbines on stability of power-system dynamics," in Proceedings of the IEEE Power & Energy Society General Meeting, Atlanta, United States of America, 04-08 August, 2019.

[8] A. K. Gupta, A. Shukla, K. Verma, and K. R. Niazi, "Dynamic impact analysis of wind integration on small signal stability of power system," in Proceedings of the International Conference on Power Electronics & IoT Applications in Renewable Energy and its Control, Mathura, India, 28-29 February, 2020.

[9] L. Shi, S. Sun, L. Yao, Y. Ni, and M. Bazargan, "Effects of wind generation intermittency and volatility on power system transient stability," *IET Renewable Power Generation,* vol. 8, no. 5, pp. 509-521, 2013.

[10] W. Wu, K. Wang, G. Li, and Y. Hu, "A stochastic model for power system transient stability with wind power," in Proceedings of the IEEE PES General Meeting, Conference & Exposition, National Harbor, United States of America, 27-31 July , 2014.

[11] Z. Yue, Y. Liu, Y. Yu, and J. Zhao, "Probabilistic transient stability assessment of power system considering wind power uncertainties and correlations," *Electrical Power and Energy Systems,* vol. 117, no. 2020, pp. 1-11, 2020.

[12] H. Silva-Saravia, and H. Pulgar-Painemal, "Effect of wind farm spatial correlation on oscillation damping in the WECC system," in Proceedings of the North American Power Symposium, Wichita, United States of America, 13-15 October, 2019.

[13] J. Xu, W. Wu, K. Wang, and G. Li, "C-Vine pair copula based wind power correlation modelling in probabilistic small signal stability analysis," *IEEE/CAA Journal of Automatica Sinica,* vol. 7, no. 4, pp. 1154-1160, 2020.

[14] P. Kundur, *Power system stability and control*. New York: McGraw-Hill, 1994.

[15] M. El-Shimy, N. Mostafa, A. Afandi, N, A. Sharaf, M, and M. Attia, A, "Impact of load models on the static and dynamic performances of grid-connected wind power plants: a comparative analysis," *Mathematics and Computers in Simulation,* vol. 149, no. 1, pp. 91-108, 2018.

[16] M. Sanaye-Pasand, H. Seyedi, H. Lesani, and M. Dadashzadeh, "Simulation and analysis of load modelling effects on power system transient stability," *Mathematische Annalen,* vol. 12, no. 2, pp. 180-201, 2005.

[17] E. Vittal, P. Cuffe, and A. Keane, "Transient stability impacts from distribution connected wind farms," in Proceedings of the IEEE Power and Energy Society General Meeting, San Diego, United States of America, 22-26 July, 2012.

[18] E. Vittal, M. O'Malley, and A. Keane, "Rotor angle stability with high penetrations of wind generation," *IEEE Transactions on Power Systems,* vol. 27, no. 1, pp. 353-362, 2012.

[19] L. Shi, S. Dai, L. Yao, Y. Ni, and M. Bazargan, "Impact of wind farms of DFIG type on power system transient stability," *Journal of Electromagnetic Analysis and Applications,* vol. 2, no. 8, pp. 475-481, 2010.

[20] M. A. Chowdhury, N. Hosseinzadeh, W. X. Shen, and H. R. Pota, "Comparative study on fault responses of synchronous generators and wind turbine generators

using transient stability index based on transient energy function," *International Journal of Electrical Power and Energy Systems,* vol. 51, no. 1, pp. 145-152, 2013.

[21] F. S. Chassin, E. T. Mayhorn, M. A. Elizondo, and S. Lu, "Load modeling and calibration techniques for power system studies," in Proceedings of the North American Power Symposium, Boston, United States of America, 4-6 August, 2011.

[22] B. Marah, and A. O. Ekwue, "Probabilistic load flows," in Proceedings of the International Universities Power Engineering Conference, Stoke on Trent, United Kingdom, 1-4 September, 2015.

[23] Z. Qin, W. Li, and X. Xiong, "Incorporating multiple correlations among wind speeds, photovoltaic powers and bus loads in composite system reliability evaluation," *Applied Energy,* vol. 110, no. 2013, pp. 285-294, 2013.

[24] M. O. M. Mahmoud, M. Jaidane-Saidane, and N. Hizaoui, "The use of mixture of generalized Gaussian for trend analysis of the load duration curve: summer and winter load variability in Tunisia," in Proceedings of the 43rd International Universities Power Engineering Conference, Padua, Italy, 1-4 September, 2008.

[25] Y. Li, Z. Yang, G. Li, D. Zhao, and W. Tian, "Optimal scheduling of an isolated microgrid with battery storage considering load and renewable generation uncertainties," *IEEE Transactions on Industrial Electronics,* vol. 66, no. 2, pp. 1565-1575, 2019.

[26] M. T. Hagh, P. Amiyan, S. Galvani, and N. Valizadeh, "Probabilistic load flow using the particle swarm optimisation clustering method," *IET Generation, Transmission & Distribution,* vol. 12, no. 3, pp. 780-789, 2018.

[27] H. Wang,and B. Zou, "Probabilistic computational model for correlated wind speed, solar irradiation, and load using Bayesian network," *IEEE Access,* vol. 8, no. 1, pp. 51653-51663, 2020.

[28] J. Cai, Q. Xu, M. Cao, and B. Yang, "A novel importance sampling method of power system reliability assessment considering multi-state units and correlation between wind speed and load," *International Journal of Electrical Power Energy Systems,* vol. 109, no. 2019, pp. 217-226, 2019.

[29] R. Singh, B. C. Pal, and R. A. Jabr, "Statistical representation of distribution system loads using Gaussian mixture model," *IEEE Transactions on Power Systems,* vol. 25, no. 1, pp. 29-37, 2009.

[30] H. A. Pulgar-Painemal,and P. W. Sauer, "Towards a wind farm reduced-order model," *Electric Power Systems Research,* vol. 81, no. 8, pp. 1688-1695, 2011.

[31] S. G. Varzaneh, M. Abedi, and G. Gharehpetian, "A new simplified model for assessment of power variation of DFIG-based wind farm participating in frequency control system," *Electric Power Systems Research,* vol. 148, no. 1, pp. 220-229, 2017.

[32] C. Eping, J. Stenzel, M. Pöller, and H. Müller, "Impact of large scale wind power on power system stability," in Proceedings of the 5th International Workshop on Large-scale Integration of Wind Power and Transmission Networks for Offshore Wind Farms, Glasgow, Scotland, 7–8 April , 2005.

[33] S. Q. Bu, X. Zhang, S. W. Xia, Y. Xu, B. Zhou, and X. Lu, "Reducing model complexity of DFIG-based wind turbines to improve the efficiency of power system stability analysis," *Energy Procedia,* vol. 142, no. 1, pp. 971-976, 2017.

[34] M. A. Pöller, "Doubly-fed induction machine models for stability assessment of wind farms," in Proceedings of the IEEE Bologna Power Tech Conference, Bologna, Italy, 23-26 June, 2003.

[35] S. Xia, Q. Zhang, S. Hussain, B. Hong, and W. Zou, "Impacts of integration of wind farms on power system transient stability," *Applied Sciences,* vol. 8, no. 8, pp. 1-16, 2018.

[36] Y. Wu, T. Lee, T. Hsieh, and W. Lin, "Impact on critical clearing time after integrating large-scale wind power into Taiwan power system," *Sustainable Energy Technologies and Assessments,* vol. 16, no. 1, pp. 128-136, 2016.

[37] M. Edrah, K. L. Lo, and O. Anaya-Lara, "Impacts of high penetration of DFIG wind turbines on rotor angle stability of power systems," *IEEE Transactions on Sustainable Energy,* vol. 6, no. 3, pp. 759-766, 2015.

[38] A. Parajuli, "A statistical analysis of wind speed and power density based on Weibull and Rayleigh models of Jumla, Nepal," *Energy and Power Engineering,* vol. 8, no. 7, pp. 271-282, 2016.

[39] G. D. Nage, "Analysis of wind speed distribution: comparative study of Weibull to Rayleigh probability density function; a case of two sites in Ethiopia," *American Journal of Modern Energy,* vol. 2, no. 3, pp. 10-16, 2016.

[40] A. I. Idriss, A. A. Mohamed, T. C. Akinçi, R. A. Ahmed, A. I. Omar, R. Caglar, and S. Seker, "Accuracy of eight probability distribution functions for modeling wind

speed data in Djibouti," *International Journal of Renewable Energy Research,* vol. 10, no. 2, pp. 780-790, 2020.

[41] Q. Han, S. Ma, T. Wang, and F. Chu, "Kernel density estimation model for wind speed probability distribution with applicability to wind energy assessment in China," *Renewable and Sustainable Energy Reviews,* vol. 115, no. 1, pp. 1-14, 2019.

[42] B. Hu, Y. Li, H. Yang, and H. Wang, "Wind speed model based on kernel density estimation and its application in reliability assessment of generating systems," *Journal of Modern Power Systems and Clean Energy,* vol. 5, no. 2, pp. 220-227, 2017.

[43] T. Soukissian, F. Karathanasi, and F. Falcieri, "Wind speed distributions in the Italian coasts," *Renewable Energy and Power Quality Journal,* vol. 1, no. 12, pp. 26-31, 2014.

[44] E. C. Morgan, M. Lackner, R. M. Vogel, and L. G. Baise, "Probability distributions for offshore wind speeds," *Energy Conversion and Management,* vol. 52, no. 1, pp. 15-26, 2011.

[45] Y. Wang, Q. Hu, L. Li, A. M. Foley, and D. Srinivasan, "Approaches to wind power curve modeling: A review and discussion," *Renewable Sustainable Energy Reviews,* vol. 116, no. 2019, pp. 1-21, 2019.

[46] V. Sohoni, S. C. Gupta, and R. K. Nema, "A critical review on wind turbine power curve modelling techniques and their applications in wind based energy systems," *Journal of Energy,* vol. 2016, no. 1, pp. 1-18, 2016.

[47] S. Li , C. Liu, H. Yue, C. Su, C. He, and J. Wang, "Wind power correlation analysis based on mix copula," in Proceedings of the 2nd IEEE Conference on Energy Internet and Energy System Integration, Beijing, China, 20-22 October, 2018.

[48] X. Chen, J. Han, T. Zheng, P. Zhang, S. Duan, and S. Miao, "A vine-copula based voltage state assessment with wind power integration," *Energies,* vol. 12, no. 2019, pp. 1-21, 2019.

[49] Y. Wang,and Y. Luo, "Research of wind power correlation with three different data types based on mixed copula," *IEEE Access,* vol. 6, pp. 77986-77995, 2018.

[50] Q. Xiao,and S. Zhou, "Probabilistic power flow computation considering correlated wind speeds," *Applied Energy,* vol. 231, no. 2018, pp. 677-685, 2018.

[51] Y. Pan, L. Shi, and Y. Ni, "Modelling of multiple wind farms output correlation based on copula theory," *The Journal of Engineering,* vol. 2017, no. 13, pp. 2303-2308, 2017.

[52] F. Chen, H. Liu, J. Li, and X. Zhang, "Comparison of simulation methods of spatially correlated wind speeds," in Proceedings of the 5th International Conference on Electric Utility Deregulation and Restructuring and Power Technologies, Changsha, China, 26-29 November, 2015.

[53] J. Cao, and Z. Yan, "Probabilistic optimal power flow considering dependences of wind speed among wind farms by pair-copula method," *International Journal of Electrical Power and Energy Systems,* vol. 84, no. 2017, pp. 296-307, 2017.

[54] H. Louie, "Evaluating Archimedean copula models of wind speed for wind power modeling," in Proceedings of the IEEE Power and Energy Society Conference and Exposition in Africa, Johannesburg, South Africa, 9-13 July , 2012.

[55] K. A. Folly, and S. P. N. Sheetekela, "Impact of fixed and variable speed wind generators on the transient stability of a power system network," in Proceedings of the IEEE/PES Power Systems Conference and Exposition, Seattle, United States of America, 15-18 March, 2009.

[56] T. Wang, J. Yang, J. Liu, P. Gupta, A. Pal, and J. Deng, "SDAE-based probabilistic stability analysis of wind integrated power systems," in Proceedings of the 2nd IEEE Conference on Energy Internet and Energy System Integration, Beijing, China, 20-22 October, 2018.

[57] Y. Zhang, and S. Ula, "Comparison and evaluation of three main types of wind turbines," in Proceedings of the IEEE/PES Transmission and Distribution Conference and Exposition, Chicago, United States of America, 21-24 April, 2008.

[58] A. Abdulkarim, S. M. Abdelkader, D. J. Morrow, A. J. Falade, and Y. A. Adediran, "Statistical analysis of wind speed for electrical power generation in some selected sites in northern Nigeria," *Nigerian Journal of Technology,* vol. 36, no. 4, pp. 1249-1257, 2017.

[59] W. Asquith, "L-moments, censored L-moments, trimmed L-moments, L-comoments, and many distributions," 2020. Accessed: 10 April 2020. [Online]. Available: https://cran.r-project.org/web/packages/lmomco/lmomco.pdf

[60] M. J. Chihota, and C. T. Gaunt, "Impact of input model accuracy on probabilistic load flow outputs," in Proceedings of the IEEE International Conference on

Probabilistic Methods Applied to Power Systems (PMAPS), Boise, United States of America, 24-28 June, 2018.

[61] O. Moses,and B. P. Parida, "Statistical modelling of Botswana's monthly maximum wind speed using a four-parameter Kappa distribution," *American Journal of Applied Sciences,* vol. 13, no. 6, pp. 773-778, 2016.

[62] K. Kasantikul, D. Yang, and Q. Wang, "Short-term wind speed estimation based on kernel density estimation using GNSS-reflectometry observation data," in Proceedings of the International Conference on Applied System Innovation, Sapporo, Japan, 13-17 May, 2017.

[63] W. Liu,and Y. Liu, "Enabling wind farm to be black-start source by energy storage," *The Journal of Engineering,* vol. 2019, no. 18, pp. 5138-5141, 2019.

[64] P. Van Kerm, "Kernel-smoothed cumulative distribution function estimation with akdensity," *The Stata Journal,* vol. 12, no. 3, pp. 543–548, 2012.

[65] J. Raz, E. J. Fernandez, and J. Gillespie, "Modeling NMR lineshapes using Logspline density functions," *Journal of Magnetic Resonance,* vol. 127, no. 1997, pp. 173–183, 1997.

[66] M. Sahmoudi, K. Abed-Meraim, M. Lavielle, E. Kuhn, and P. Ciblat, "Blind source separation of noisy mixtures using a semi-parametric approach with application to heavy-tailed signals," in Proceedings of the 13th European Signal Processing Conference, Antalya, Turkey, 4-8 September, 2005.

[67] K. Xie, Y. Li, and W. Li, "Modelling wind speed dependence in system reliability assessment using copulas," *IET Renewable Power Generation,* vol. 6, no. 6, pp. 392-399, 2012.

[68] H. T. Zhang, K. Chang, H. Zhang, and L. L. Lai, "A novel probabilistic approach for evaluating fault ride-through capability of wind generation," in Proceedings of the International Conference on Machine Learning and Cybernetics, Jeju, South Korea, 10-13 July, 2016.

[69] M. J. Vahid-Pakdel,and B. Mohammadi-ivatloo, "Probabilistic assessment of wind turbine impact on distribution networks using linearized power flow formulation," *Electric Power Systems Research,* vol. 162, no. 1, pp. 109-117, 2018.

[70] Enercon, "Enercon product overview," 2015. Accessed: 09 March 2020. [Online]. Available: https://wind-turbine.com/download/101655/enercon_produkt_en_06_2015.pdf

[71] N. Bokde, A. Feijóo, and D. Villanueva, "Wind turbine power curves based on the Weibull cumulative distribution function," *Applied Sciences,* vol. 8, no. 1757, pp. 1-18, 2018.

[72] O. Sadeghian, A. Oshnoei, M. Kheradmandi, R. Khezri, and B. Mohammadi-Ivatloo, "A robust data clustering method for probabilistic load flow in wind integrated radial distribution networks," *International Journal of Electrical Power & Energy Systems,* vol. 115, no. 2020, p. 105392, 2020.

[73] H. Saadat, *Power system analysis*, 3rd ed. United States of America: PSA Publishing, 2010.

[74] Y. Lanzhen, and H. Minghu, "Laws of large numbers for uncertain variables," in Proceedings of the 6th International Conference on Biomedical Engineering and Informatics, Hangzhou, China, 16-18 December, 2013.

[75] S. Choudhary, and F. B. Sharma, "Small signal stability analysis of renewable source connected power system and identification of oscillatory modes using wavelet transform," in Proceedings of the International Conference on Smart Grid and Clean Energy Technologies, Offenburg, Germany, 20-23 October, 2015.

[76] B. Qi, K. N. Hasan, and J. V. Milanovic, "Identification of critical parameters affecting voltage and angular stability considering load-renewable generation correlations," *IEEE Transactions on Power Systems,* vol. 34, no. 4, pp. 2859 - 2869, 2019.

[77] Y. Zhang, S. Gao, J. Han, and M. Ban, "Wind speed prediction research considering wind speed ramp and residual distribution," *IEEE Access,* vol. 7, no. 1, pp. 131873-131887, 2019.

[78] University of Cyprus, "IEEE 9-bus modified test system." Accessed: 29 September 2020. [Online]. Available: https://www2.kios.ucy.ac.cy/testsystems/index.php/ieee-9-bus-modified-test-system/

[79] C. W. Taylor, *Power system voltage stability*, 1 st ed., Singapore: McGraw-Hill, 1994.

[80] A. A. Sallam, and O. P. Malik, *Power system stability: modelling, analysis and control,* Series 76, London: The Institution of Engineering and Technology, 2015.

[81] IEEE, "IEEE guide for synchronous generator modelling practices and applications in power system stability analyses," New York, IEEE Std 1110, 2003.

[82] Digsilent Powerfactory, "P*owerFactory 2020 technical reference documentation: synchronous machine*," Revision 2, Gomaringen, 17 June 2020.

[83] M. R. Mathur,and R. K. Varma, *Thyristor-based FACTS controllers for elerctrical transmission systems*, 1st ed. New York: John Wiley & Sons, 2002.

[84] IEC, "Wind turbines - part 27-1: electrical simulation models - wind turbines," International Electrotechnical Commission (IEC), IEC 61400-27-1:2015, October 2015.

[85] *Grid connection code for renewable power plants (RPPs) connected to the electricity transmission system (TS) or distribution system (DS) in South Africa* National Energy Regulator of South Africa, January 2022. [Online]. Available: https://www.nersa.org.za/wp-content/uploads/bsk-pdf-manager/2022/01/SAGC-Requirements-for-Renewable-Power-Plants-Rev-3.1.pdf

[86] S. L. A. Sardinha, S. J. N. Cisneiros, M. J. Botelho, P. Gomes, D. O. C. Brasil, F. C. Medeiros, A. Bianco, A. D. R. Medeiros, P. E. M. Quintao, A. A. Barbosa, and F. R. Sobral, "Improvement of technical requirements for connecting wind plants in the Brazilian interconnected power system," in Proceedings of the 46 CIGRE Session, Paris, France, 21-26 August, 2016.

[87] R. Villena-Ruiz, A. Honrubia-Escribano, J. Fortmann, and E. Gómez-Lázaro, "Field validation of a standard Type 3 wind turbine model implemented in DIgSILENT-PowerFactory following IEC 61400-27-1 guidelines," *Electrical Power & Energy Systems,* vol. 116, no. 2020, pp. 1-15, 2020.

APPENDIX A: IEEE 9-BUS TEST SYSTEM PARAMETERS

Table A.1: IEEE 9-bus test system synchronous generator GENROU dynamic model data

Quantity	G1	G2	G3
H(s)	2.6312	4.1296	4.768
D	2	2	2
ra (pu)	0.004	0.0016	0.004
xd (pu)	1.7	1.7	1.22
xq (pu)	1.65	1.62	1.16
$x'd$ (pu)	0.27	0.256	0.174
$x'q$ (pu)	0.47	0.245	0.25
$x''d$ (pu)	0.2	0.185	0.134
$x''q$ (pu)	0.2	0.185	0.134
$xl\ or\ xp$ (pu)	0.16	0.155	0.0078
$T'd0$ (s)	3.8	4.8	8.97
$T'q0$ (s)	0.48	0.5	0.5
$T''d0$ (s)	0.01	0.01	0.033
$T''q0$ (s)	0.0007	0.0007	0.07
$S(1.0)$	0.09	0.125	0.1026
$S(1.2)$	0.4	0.45	0.432

Table A.2: IEEE 9-bus test system synchronous generator IEEET1 exciter model data

Quantity	G1	G2	G3
Tr (s)	0	0	0.06
Ka (pu)	200	30	25
Ta (s)	0.395	0.4	0.2
Ke (pu)	1	-0.02	-0.0601
Te (s)	0	0.56	0.6758
Kf (pu)	0.0635	0.05	0.108
Tf (s)	1	1.3	0.35
E1 (pu)	2.88	2.5875	2.4975
Se1 (pu)	0	0.7298	0.0949
E2 (pu)	3.84	3.45	3.33
Se2 (pu)	0	1.3496	0.37026
Vrmin (pu)	-3.84	-4.59	-1
Vrmax (pu)	3.84	4.59	1

Table A.3: IEEE 9-bus test system synchronous generator BPA_GG governor system model data

Quantity	G1	G2	G3
T2 (s)	0.05	0	0
T1 (s)	0.15	0.1	0.083
K1 (pu)	1	1	1
T (s)	0	0	0
R (pu)	0.00976	0.01852	0.04
T3 (s)	0.3	0.259	0.2
F5 (pu)	0.27	0.272	0.28
B (s)	1	1	1
T5 (s)	8	10	5
K2 (pu)	1	1	1
T4 (s)	0.26	0.1	0.05
PN (MW)	0	0	0
D	2	2	2
Pinitial (pu)	0.155663	0.710894	0.802105
Pmin (pu)	0	0	0
Pmax (pu)	0.8984	0.8518	1.056

APPENDIX B: WIND POWER GENERATORS' REACTIVE POWER RESPONSE DURING SYSTEM FAULTS

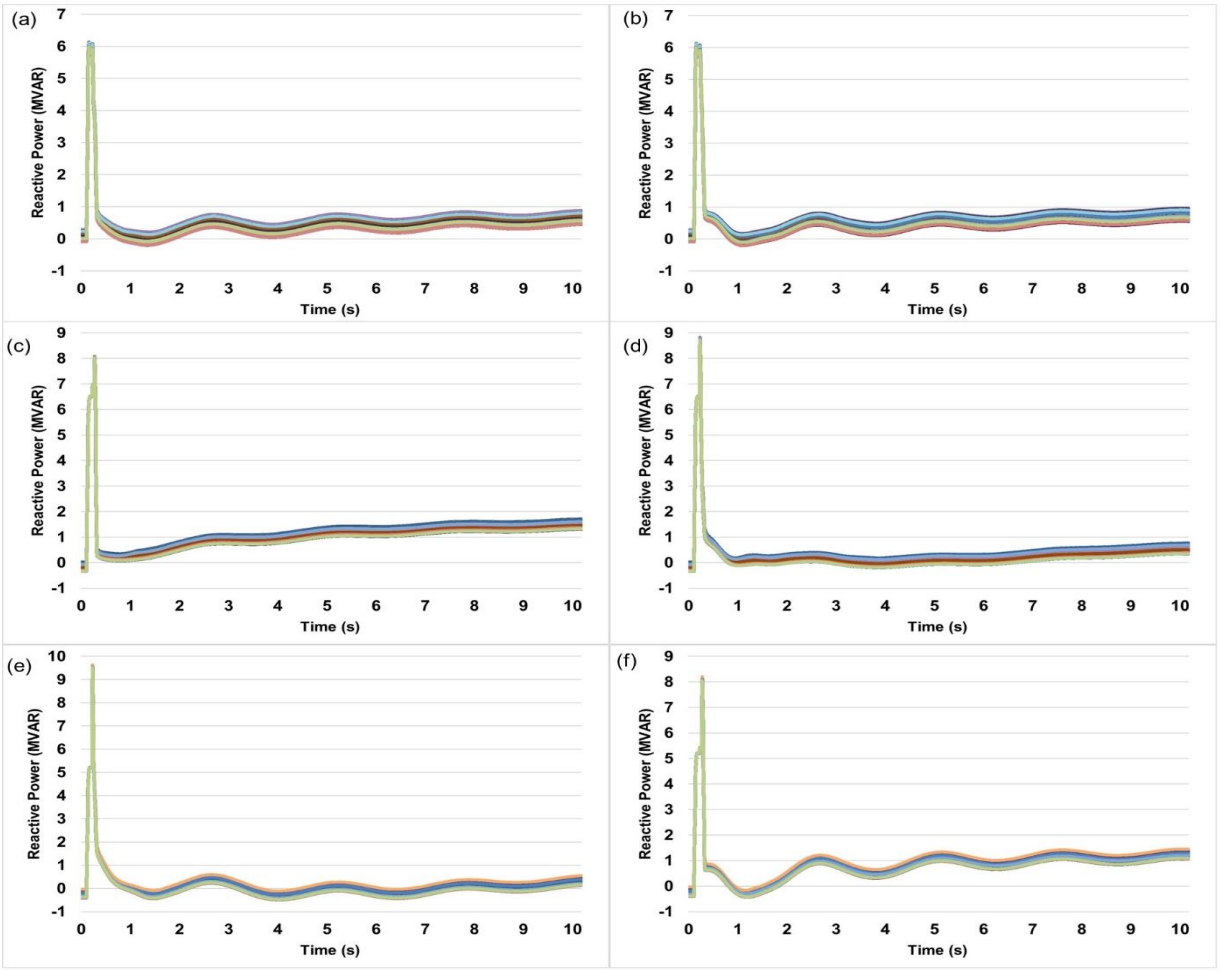

Figure B1: WPGs' reactive power injection with power production developed using wind speed modelled by the Weibull distribution function: (a) WPG1 reactive power with the fault applied on line 6-9, (b) WPG1 reactive power with the fault applied on line 8-9, (c) WPG2 reactive power with the fault applied on line 6-9, (d) WPG2 reactive power with the fault applied on line 8-9, (e) WPG3 reactive power with the fault applied on line 6-9, and (f) WPG3 reactive power with the fault applied on line 8-9

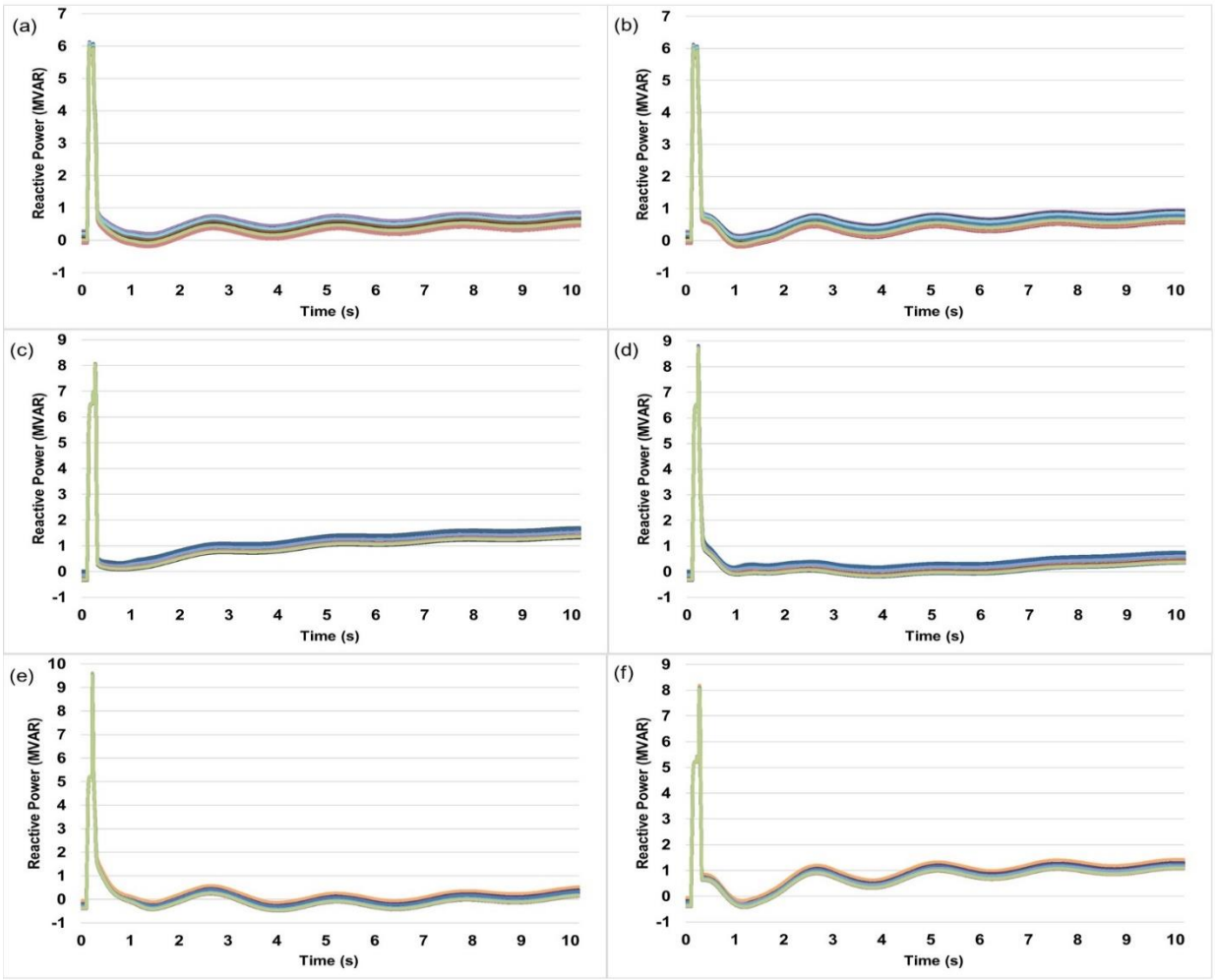

Figure B2: WPGs' reactive power injection with power production developed using wind speed modelled by the Rayleigh distribution function: (a) WPG1 reactive power with the fault applied on line 6-9, (b) WPG1 reactive power with the fault applied on line 8-9, (c) WPG2 reactive power with the fault applied on line 6-9, (d) WPG2 reactive power with the fault applied on line 8-9, (e) WPG3 reactive power with the fault applied on line 6-9, and (f) WPG3 reactive power with the fault applied on line 8-9

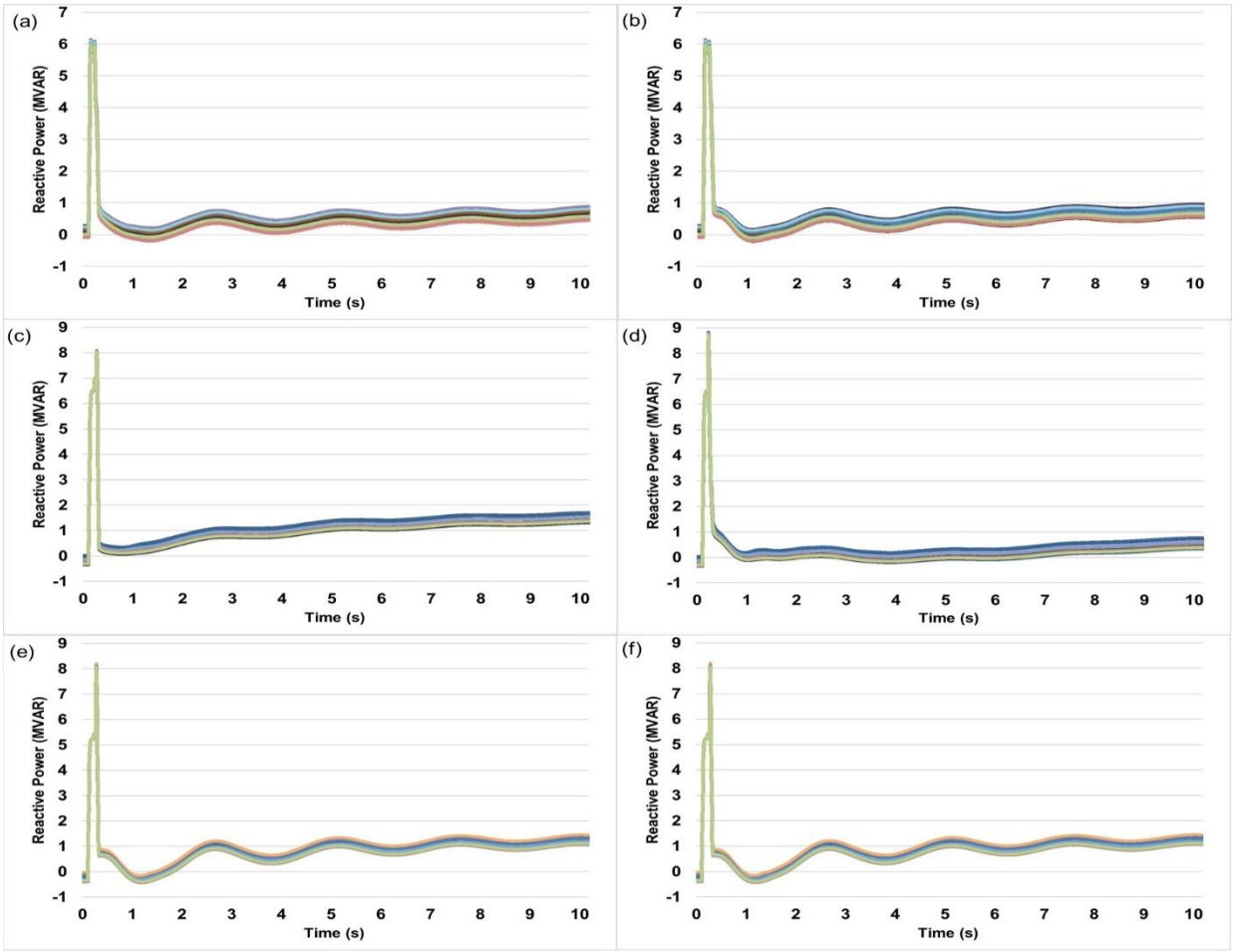

Figure B3: WPGs' reactive power injection with power production developed using wind speed modelled by the Gumbel distribution function: (a) WPG1 reactive power with the fault applied on line 6-9, (b) WPG1 reactive power with the fault applied on line 8-9, (c) WPG2 reactive power with the fault applied on line 6-9, (d) WPG2 reactive power with the fault applied on line 8-9, (e) WPG3 reactive power with the fault applied on line 6-9, and (f) WPG3 reactive power with the fault applied on line 8-9

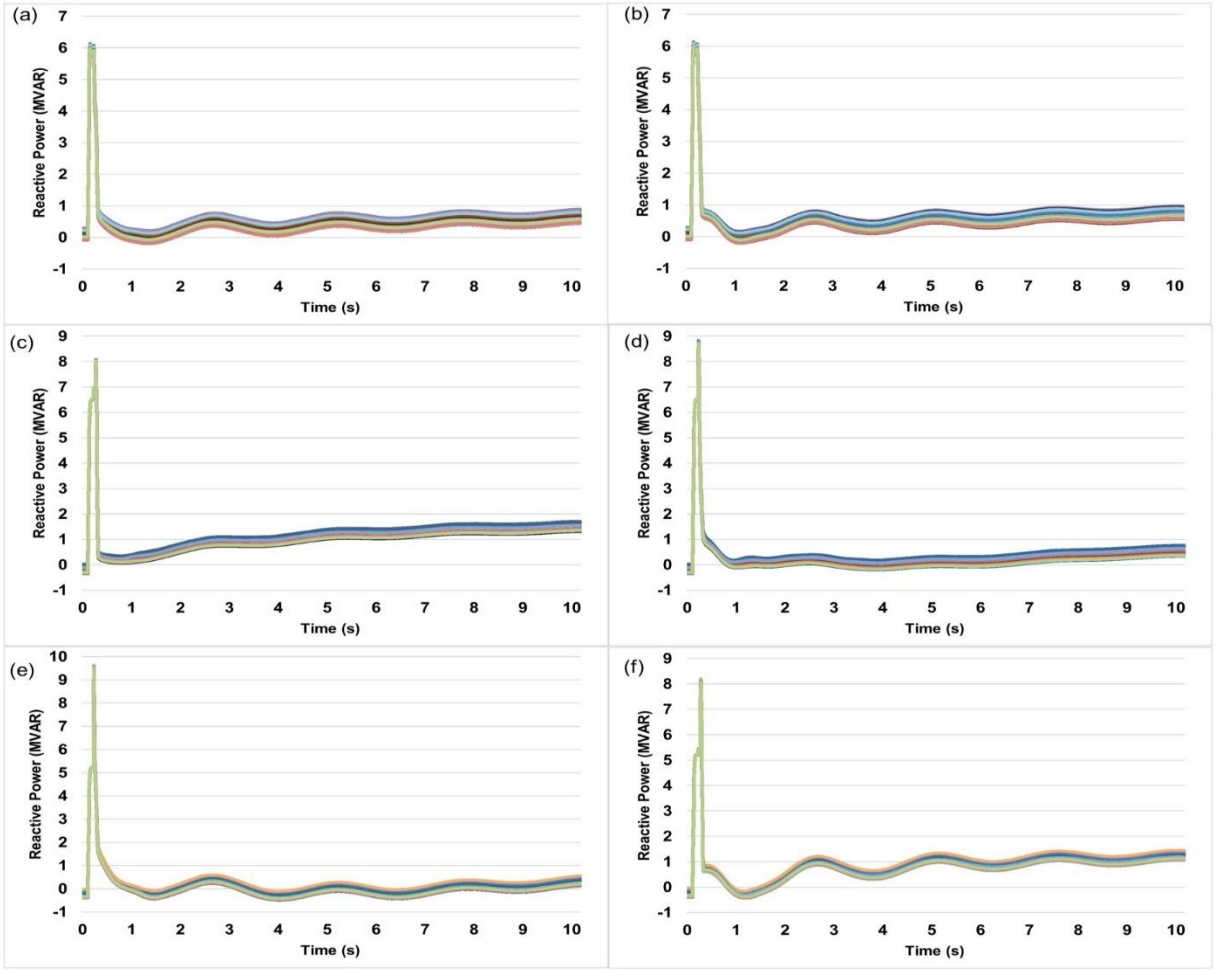

Figure B4: WPGs' reactive power injection with power production developed using wind speed modelled by the Wakeby distribution function: (a) WPG1 reactive power with the fault applied on line 6-9, (b) WPG1 reactive power with the fault applied on line 8-9, (c) WPG2 reactive power with the fault applied on line 6-9, (d) WPG2 reactive power with the fault applied on line 8-9, (e) WPG3 reactive power with the fault applied on line 6-9, and (f) WPG3 reactive power with the fault applied on line 8-9

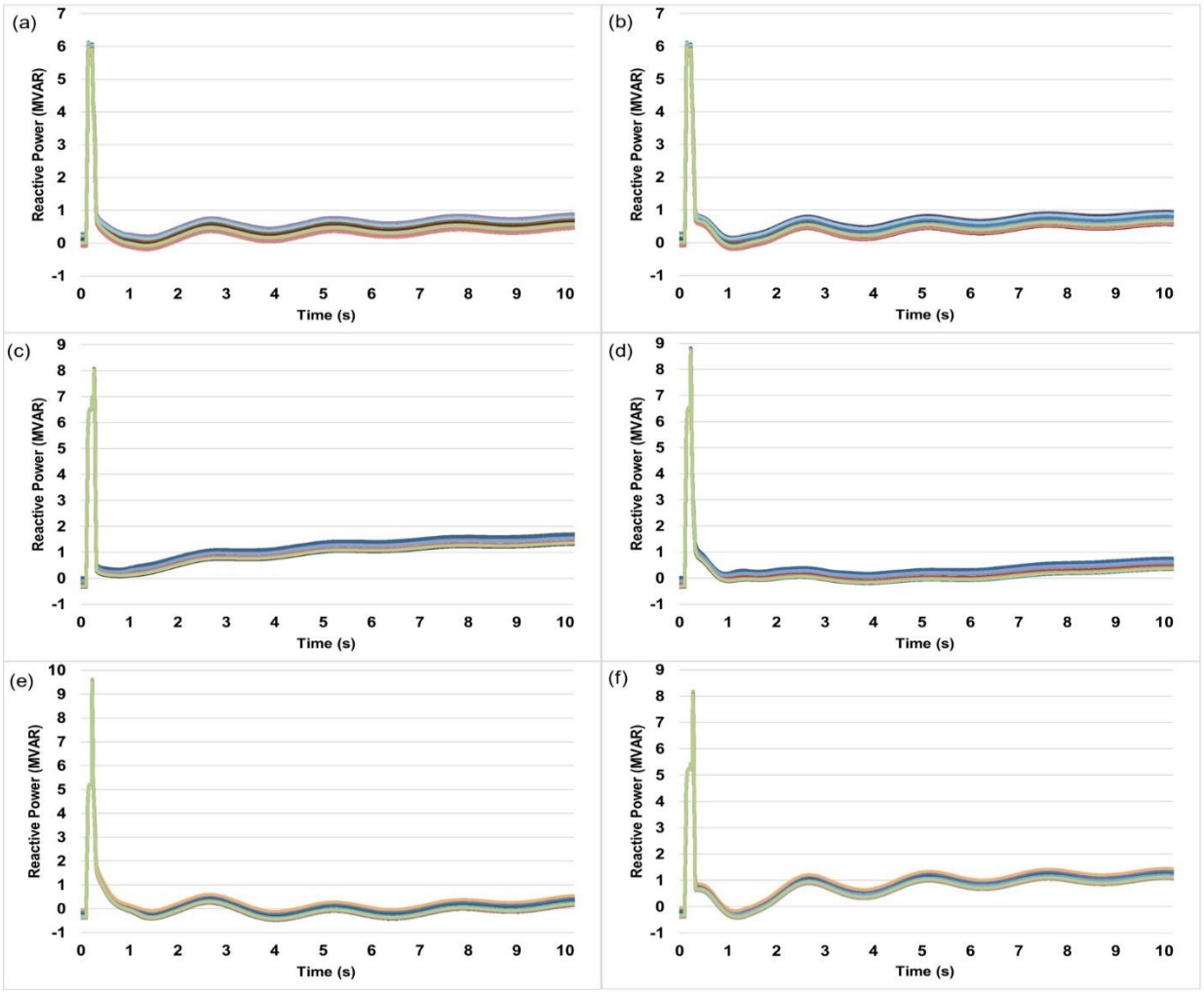

Figure B5: WPGs' reactive power injection with power production developed using wind speed modelled by the Kappa distribution function: (a) WPG1 reactive power with the fault applied on line 6-9, (b) WPG1 reactive power with the fault applied on line 8-9, (c) WPG2 reactive power with the fault applied on line 6-9, (d) WPG2 reactive power with the fault applied on line 8-9, (e) WPG3 reactive power with the fault applied on line 6-9, and (f) WPG3 reactive power with the fault applied on line 8-9